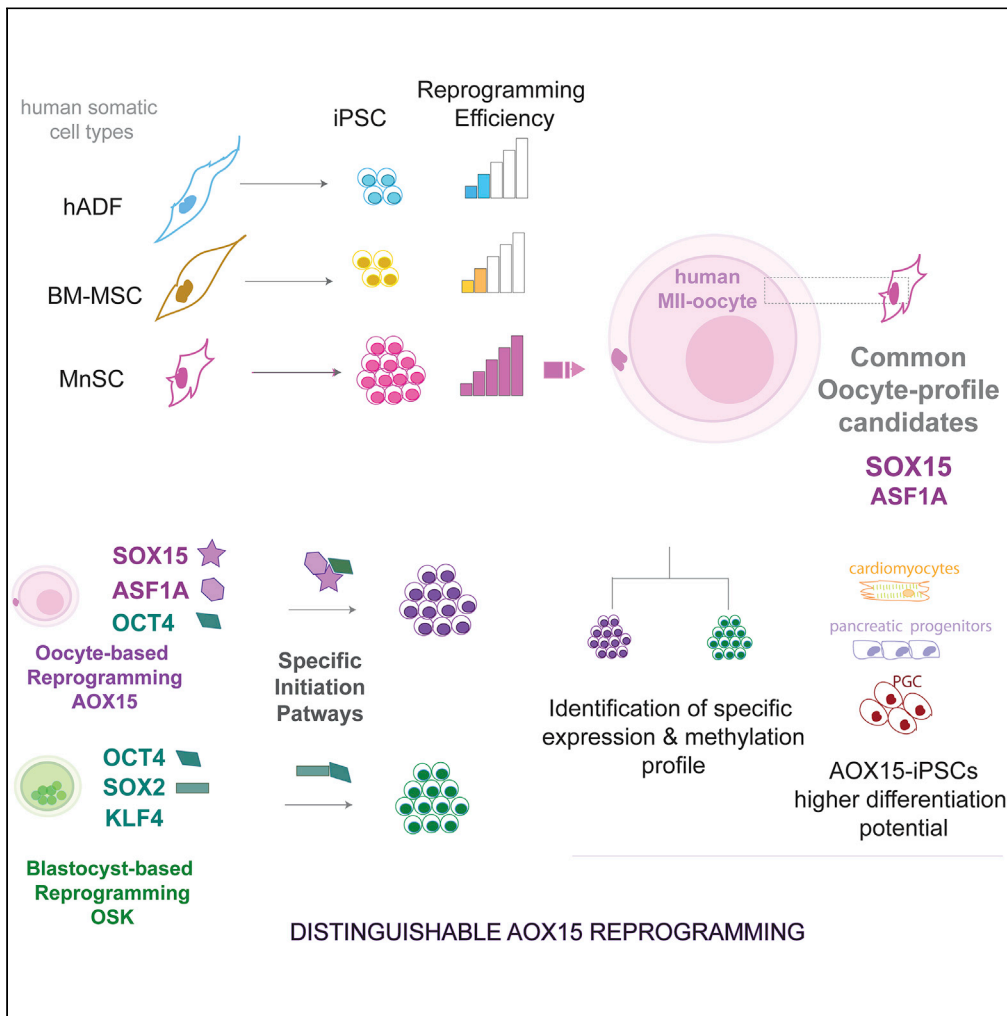**Article**

# Analysis of Menstrual Blood Stromal Cells Reveals SOX15 Triggers Oocyte-Based Human Cell Reprogramming

Lidia Lopez-Caraballo, Jordi Martorell-Marugan, Pedro Carmona-Saez, Elena Gonzalez-Muñoz

egonmu@uma.es

## HIGHLIGHTS

MnSC expression signature reveals SOX15 as a crucial oocyte-enriched reprogramming factor

SOX15 orchestrates an efficient oocyte-based reprogramming combination in MnSC

Oocyte-based reprogrammed iPSCs (AOX15) show distinct pluripotent state

AOX15 iPSCs present higher differentiation capacity than OSKM-iPSCs

**Article**

# Analysis of Menstrual Blood Stromal Cells Reveals SOX15 Triggers Oocyte-Based Human Cell Reprogramming

Lidia Lopez-Caraballo,[1] Jordi Martorell-Marugan,[2,5] Pedro Carmona-Saez,[2,6] and Elena Gonzalez-Muñoz[1,3,4,7,*]

## SUMMARY

**Cell reprogramming has revolutionized cell and regenerative biology field. However, human iPS derivation remains inefficient and variable. A better knowledge of molecular processes and the rationale underlying the importance of somatic cell origin is crucial to uncover reprogramming mechanisms. Here, we analyze the molecular profile of different human somatic cell types. We show menstrual blood-derived stromal cells (MnSCs) have a distinct, reprogramming prone, profile, and we identify SOX15 from their oocyte-related signature as a prominent responsible candidate. SOX15 orchestrates an efficient oocyte-based reprogramming combination when overexpressed with the also oocyte-enriched histone chaperone ASF1A and OCT4 and, through specific mechanism, generates iPSCs with distinguishable pluripotent state that further present higher differentiation capacity than canonical iPSCs. Our work supports the presence of different pluripotency states in reprogramming and the importance of using metaphase-II oocyte and MnSCs information to provide alternative reprogramming combinations and, importantly, to improve and understand pluripotency acquisition.**

## INTRODUCTION

Generation of induced pluripotent stem cells (iPSCs) is a complex process, and molecular mechanisms are not fully understood.

The great majority of iPSC lines have been generated from dermal fibroblasts. Nonetheless, a multitude of other cell types have been used (Patel and Yang, 2010) as bone marrow mesenchymal stromal cells (BM-MSCs) (Ohnishi et al., 2011; Park et al., 2008; Shao et al., 2012; Streckfuss-Bomeke et al., 2012). Of note, another mesenchymal cell type, menstrual blood stromal cells (MnSCs), has appeared recently in the reprogramming field with clear advantages in accessibility, and their efficiency potential has not been deeply studied (de Carvalho Rodrigues et al., 2012; Li et al., 2012).

Mammalian metaphase-II (MII) oocyte has widely been shown to have an unpaired reprogramming capacity (Gonzalez-Munoz and Cibelli, 2018; Jullien et al., 2014). By analyzing its specific factors (Assou et al., 2006, 2009; Kocabas et al., 2006) we have previously identified the histone-chaperone ASF1A as crucial for human pluripotency and have shown that overexpression of just ASF1A and OCT4 in human adult dermal fibroblast (hADFs) exposed to GDF9 can reprogram AO9-iPSCs, although noteworthy less efficiently than canonical OSKM (OCT4, SOX2, KLF4, and c-MYC) combination (Gonzalez-Munoz et al., 2014).

Sex-determining region Y-box 15 (SOX15) is a member of the SOX family of transcription factors that is highly expressed in mouse blastocyst ICM and mESCs (Maruyama et al., 2005; Yoshikawa et al., 2006), as well as in human ESCs (Pacini et al., 2010), although its expression is significantly higher in MII oocyte (Assou et al., 2006, 2009; Awe and Byrne, 2013; Kocabas et al., 2006).

Although *in vitro* analysis modeling indicates SOX15 cooperates with OCT4 on the canonical DNA element (Ng et al., 2012), mouse reprogramming assays (Nakagawa et al., 2008) and SOX15 knockout data (Lee et al., 2004; Meeson et al., 2007) suggested SOX15 has a secondary role during mouse development, and whether it participates in human reprogramming regulation and pluripotency remains elusive.

[1]Andalusian Laboratory of Cell Reprogramming (LARCel), Andalusian Centre for Nanomedicine and Biotechnology-BIONAND, Málaga 29590, Spain

[2]Bioinformatics Unit. GENYO, Centre for Genomics and Oncological Research: Pfizer/University of Granada/Andalusian Regional Government, PTS Granada, Granada E-18016, Spain

[3]Department of Cell Biology, Genetics and Physiology, University of Malaga, Málaga 29071, Spain

[4]Networking Research Center on Bioengineering, Biomaterials and Nanomedicine, (CIBER-BBN), Málaga 29071, Spain
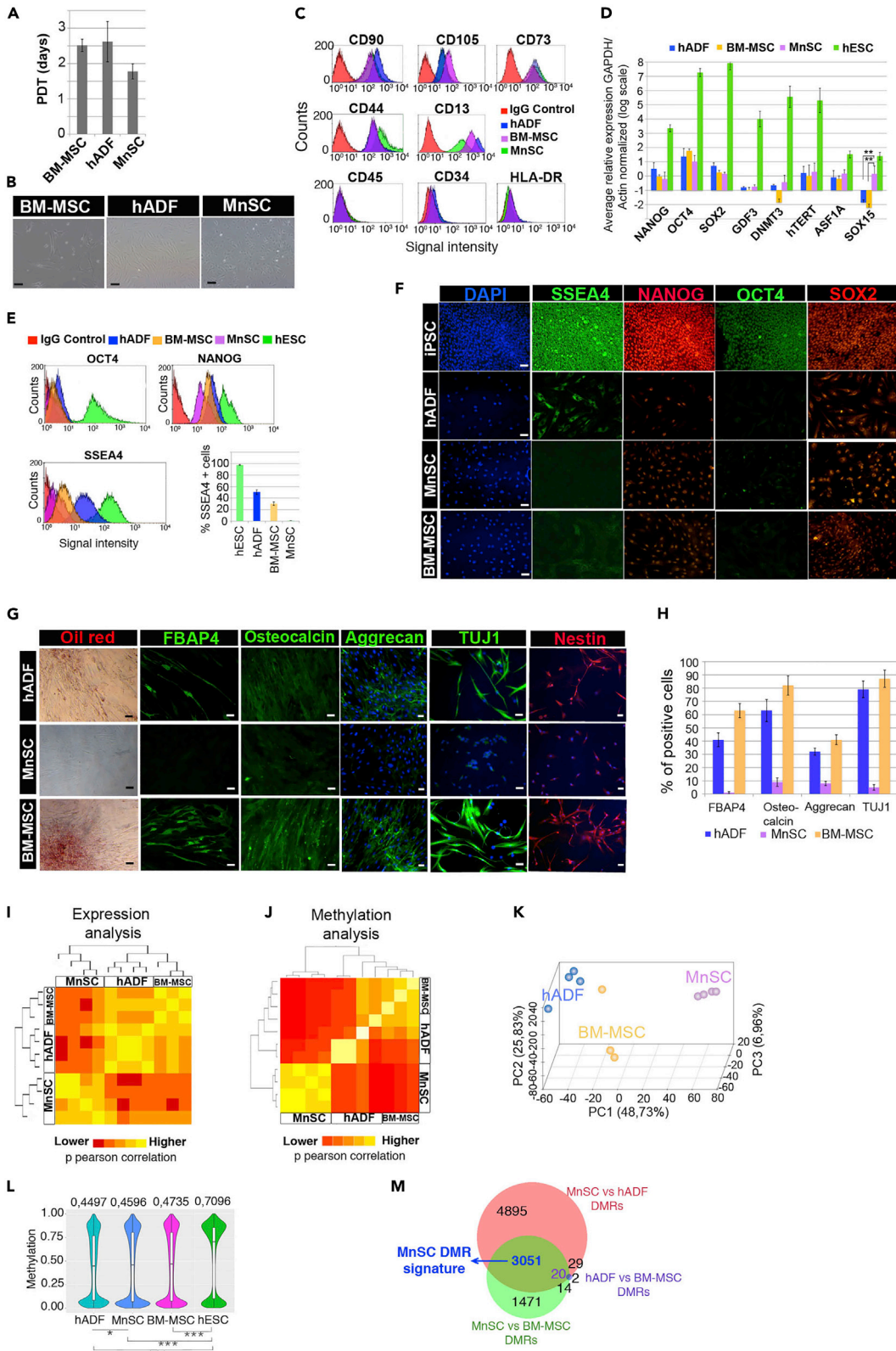
[5]Atrys Health, Barcelona, Spain

[6]Department of Statistics. University of Granada, Spain

[7]Lead Contact

*Correspondence: egonmu@uma.es

https://doi.org/10.1016/j.isci.2020.101376

**Figure 1. Somatic Cell Lines Characterization**

Adult human primary BM-MSC, hADF, and MnSC cell lines derived from three different donors were used.

(A) Average population doubling time (PDT) of the different cell lines (days). Each counting was done by triplicate during four subculture rounds.

(B) Representative bright-field images of adult human primary cell lines (scale bar, 100 μm).

(C) Histograms of flow cytometry analysis using mesenchymal markers.

(D) qRT-PCR for genes characteristic of pluripotent cells was performed as indicated on mRNA collected from hADFs, BM-MSCs, MnSCs, and H9-hESCs. Values indicate average relative expression of the specific gene normalized to GAPDH/Actin in a logarithmic scale. Data correspond to the average of three independent experiments done in triplicate with cells from three different donors (n = 9, mean values ±SEM). Student's t test was applied for statistical significance: **$p < 0.01$.

(E) Histograms of flow cytometry analysis in all somatic cell types compared with pluripotent H9-hESCs, using pluripotent cell markers fluorescent labeling. Percentage of SSEA4-positive cells was calculated from three independent experiments (three donors/cell type).

(F) Immunochemistry analysis of pluripotent markers on the different human somatic cell lines, and H9-hESCs as positive expression control (scale bar, 30 μm).

(G) Immunocytochemistry analysis of specific markers of adipogenic (FBAP4 and oil-red staining), osteogenic (Osteocacin), chondrogenic (Aggrecan), and neural (Nestin, Tuj1) differentiation 21 days after specific differentiation (scale bar, 30 μm).

(H) Quantification of the number of positive cells for each differentiated cell type from 30 images as in (G). Data correspond to the average of three independent immunochemistry experiments done in duplicate with cells from three different donors/cell type (mean values ± SEM).

(I) Correlation heatmap showing the clustering of somatic cell lines (four cell lines obtained from four different donors, except for BM-MSCs where three of the donors were used) using the RNA expression (array-based) data. Euclidean distance and complete agglomeration method were used to compute the heatmap's dendrogram. Correlation was computed with Pearson's method.

(J) Correlation heatmap showing the clustering of genome methylation analysis of somatic cell lines (as in I). Euclidean distance and complete agglomeration method were used to compute the heatmap's dendrogram.

(K) PCA analysis using methylation data as in (J).

(L) Violin plots showing the distribution of the DNA methylation (beta values) in each of the somatic samples and pluripotent hESCs. Data correspond to the average from same four different donors/cell type. Differential global methylation significance is shown (p values: ***$p < 0.001$, *$<0.05$). Median beta-values of each cell population are indicated at the top.

(M) Differentially methylated regions (DMRs) among somatic groups were used to generate Venn diagrams to identify specific and common methylated genomic regions in each pluripotent group. We have highlighted in blue the number of specific MnSC DMRs when compared with both hADF and BM-MSC. See also Figure S1.

Here we deeply characterize somatic cells to analyze factors involved in the higher reprogramming efficiency we found in MnSC. We have identified SOX15 as a crucial factor that assembles a reprogramming detonator, together with ASF1A and OCT4 (AOX15), and through specific pathways generates a distinctive pluripotent state, with superior differentiation potential. Our study provides evidence of the importance of using oocyte information to make progress of significance into pluripotency and reprogramming understanding.

## RESULTS

### MnSCs Show Distinct Expression and Epigenetic Profile and Higher iPSC Reprogramming Efficiency when Compared with hADFs and BM-MSCs

We first characterized the above-mentioned three accessible adult cell types. MnSCs have the highest proliferation rate (Figure 1A) and different morphological appearance, smaller and less spindly (Figure 1B) than hADFs and BM-MSCs. Flow cytometry analysis confirmed the expression of MSC markers, although with different mean fluorescence intensity depending on the cell type (Figure 1C).

We next evaluated the expression of pluripotency markers. Quantitative RT-PCR results confirmed expected lower expression in all somatic cell lines versus pluripotent hESCs (Figure 1D). Flow cytometry and immunofluorescence analysis revealed negligible OCT4 and SOX2 staining compared with hESCs and mild NANOG protein expression. Among somatic cell lines, hADFs showed the highest SSEA4 labeling and MnSCs the lowest (Figures 1E and 1F).

We then evaluated mesenchymal multipotency performing *in vitro* adipogenic, osteogenic, chondrogenic, and neural differentiation. MnSCs were unable to differentiate, whereas hADF and specially BM-MSC efficiently differentiate to all four lineages (Figures 1G and 1H).

Hierarchical dendrogram based on global transcription profile show MnSCs cluster together and separately to BM-MSCs and hADFs (Figure 1I). Whole-genome CpG DNA methylation analysis with unsupervised hierarchical clustering and principal component analysis (PCA) confirmed the same segregation pattern where MnSCs differ the most (Figures 1J and 1K). Global analysis of methylation profiles (GAMP)
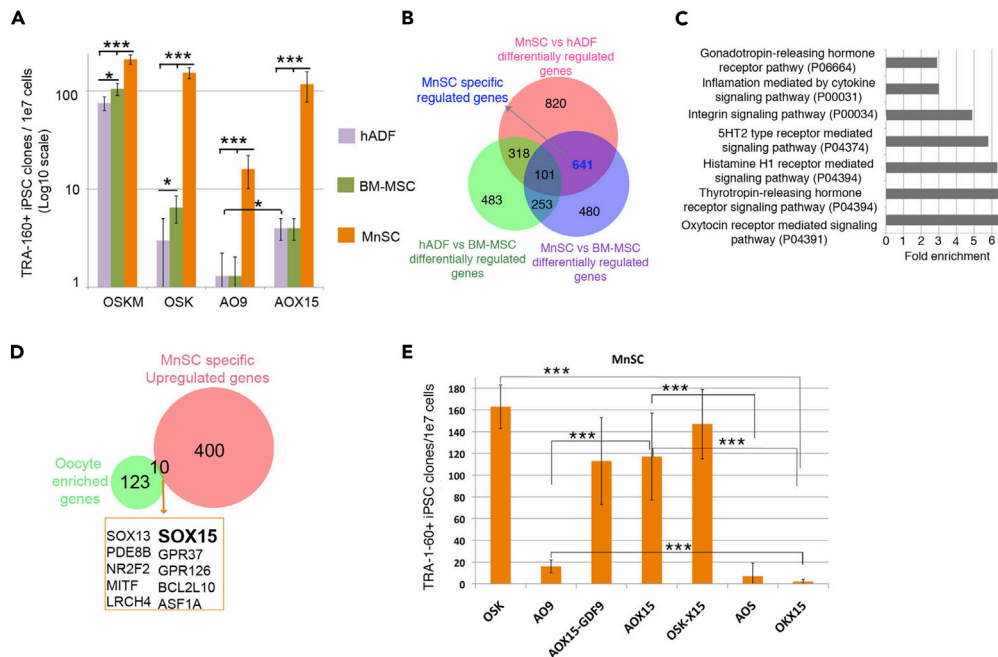
**Figure 2. MnSCs Expression Signature Reveals SOX15 as Crucial Oocyte-Enriched Reprogramming Factor**

(A) Average number of TRA-1-60+ reprogrammed iPSC lines derived from $10^7$ transduced hADFs, BM-MSCs, or MnSCs with the different factor combinations. Mean values (n = 9, triplicates with cells from three different donors/cell type) $\pm$ SEM are plotted. TRA-1-60+ reprogrammed iPSC lines were considered those that showed TRA-160+ labeling after at least five expansion passages from initial colony appearance. Student's t test was applied for statistical significance: ***p < 0.001, *<0.05 between compared groups.

(B) High-throughput array-based expression analysis of MnSC, BM-MSCs, and hADFs. Differentially regulated genes among groups were used to generate Venn diagrams to identify specific and common regulated genes in each group. We have highlighted in blue the number of specific MnSC differentially regulated genes when compared with both hADF and BM-MSC.

(C) Significant enriched gene ontologies (GO)-key PANTHER pathways (30)-(FDR p < 0.05) associated with MnSCs-specific regulated genes are shown. No GO-key PANTHER pathway with statistically significant results was found for hADF specific regulated genes and only glycolysis pathway (TPI1, PGK1, ALDOA, ENO2, and GPI) for BM-MSCs (fold enrichment 23.43, FDR $9.19 \times 10^{-4}$).

(D) Venn diagrams showing common genes among MnSCs specific upregulated genes and published lists of oocyte-enriched genes. Representative oocyte-enriched genes are highlighted. When we compared either hADFs or BM-MSCs specific overexpressed genes with available lists of highly specific oocyte factors we found no common genes among lists.

(E) Average number of TRA-1-60+ reprogrammed iPSC lines derived from 107 transduced MnSCs with the different factor combinations. Mean values (n = 9 triplicates with cells from three different donors) $\pm$ SEM are plotted. TRA-1-60+ reprogrammed iPSC lines where considered as in Figure 1A. No colonies were found when ASF1A and OCT4 (AO) combination was used. Student's t test was applied for statistical significance: ***p < 0.001 between compared groups.

indicates a significant difference in MnSCs versus hADFs (p value < 0.05) (Figure 1L). Venn diagrams showing differential methylation regions (DMRs) among somatic groups also identify their unique epigenetic profile (Figure 1M, Table S1).

These results indicate that, although all three cell types show general mesenchymal characteristics, they have different expression and epigenetic signatures, and MnSCs have the most distinct surface marker expression, methylation profile, low pluripotency genes expression, including SSEA4, and less differentiation potential.

We then analyzed iPSC generation potential. MnSCs showed the highest reprogramming efficiency using both canonical—OSKM or OSK (without c-MYC)—(~20-fold higher) and AO9 combinations (~10-fold higher). BM-MSCs present similar AO9- and higher OSKM- and OSK-reprogramming capacity than hADFs (Figure 2A).

### MnSC Expression Signature Reveals SOX15 as a Crucial Oocyte-Enriched Reprogramming Factor

To define the MnSCs gene expression signature, we identified their specific regulated genes (Figure 2B and Table S1). Gene ontology (GO) analysis revealed a significant enrichment of PANTHER pathways related to the oocyte biology (Figure 2C).

We compared MnSCs-specific overexpressed genes with available lists of highly specific oocyte factors (Assou et al., 2006, 2009; Kocabas et al., 2006) and identified SOX15 as an outlined common gene (Figure 2D). We confirmed SOX15 (Figures S1A–S1C) and ASF1A (Figures S1D and S1E) higher protein overexpression in MnSC over hADFs.

We hypothesized that the oocyte-related expression profile of MnSCs contributes to their high reprogramming efficiency and that overexpression of specific master genes of such signature could contribute to reprogramming initiation. ASF1A fulfills this concurrence, being part of the MnSC signature (Figure 2D) and oocyte-based reprogramming factor (Gonzalez-Munoz et al., 2014); we therefore investigated SOX15.

SOX15 overexpression increased more than 7-fold AO9 reprogramming (Figure 2E) in MnSCs. When we used SOX15, GDF9 is no longer needed for reprogramming, and it does not enhance SOX15-ASF1A-OCT4 (AOX15) efficiency (Figure 2E), suggesting SOX15 overexpression improves GDF9 signaling effect in reprogramming efficiency.

We have therefore identified SOX15 from the oocyte-related MnSCs signature as a reprogramming factor responsible for increased oocyte-based reprogramming combination efficiency.

### Reprogramming Occurs through Different Mechanisms and Pathways Depending on Triggering Combination

To gain insight into the mechanism underlying SOX15 role in pluripotency acquisition, we analyzed gene and protein expression showing that SOX15, but not ASF1A, is upregulated early during OSK reprogramming (Figures 3A–3D), whereas its expression decreases during spontaneous differentiation of iPSCs (Figure S4A).

SOX15 overexpression along with OCT4, SOX2, and KLF4 did not affect reprogramming efficiency; however, SOX15 combination with OCT4 and KLF4 (OKX15) strongly reduced it (over 95% reduction). Similarly, SOX2 overexpression with OCT4 and ASF1A (AOS) dramatically decreased iPSC formation (over 90% decrease) (Figure 2E).

Our results indicate SOX15 cannot replace SOX2 during OSK human reprogramming, and vice versa, SOX2 cannot replace SOX15 during AOX15 reprogramming, suggesting described factor combinations function differently and SOX15 exerts a reprogramming triggering effect only when ASF1A is also overexpressed.

To further study the signaling involved in the initiation of reprogramming we analyzed global gene expression profiles of MnSCs 5 days after factors overexpression—OSK, AOX15, and AO9—(Figure 3E and Table S2). Venn diagrams show regulation of different sets of genes. AOX15 includes AKT and ERK phosphorylation regulators BST2 and BST1, TGF-beta signaling regulators SMAD6 or SMAD1, or key mediators of interferon signaling STAT1 and STAT2. Our results show OSK and AOX15 reprogramming onset operate through different initiating pathways.

Both OSK and AOX15 combinations lead to decreased proliferation rate as a consequence of reprogramming initiation, as SOX15 and ASF1A plus SOX15 overexpression did not affect proliferation rate (Figure S2A).

We then questioned the next steps during the reprogramming process. We analyzed the expression of mesenchymal-epithelial transition (MET)/cell adhesion markers before iPSC colonies appear (days 10 and 18) (Figures S2B and S2C) and confirmed both OSK and AOX15 upregulate MET genes, supporting previous studies showing this transition as crucial for reprogramming (Buganim et al., 2013; Li et al., 2010; Subramanyam et al., 2011).
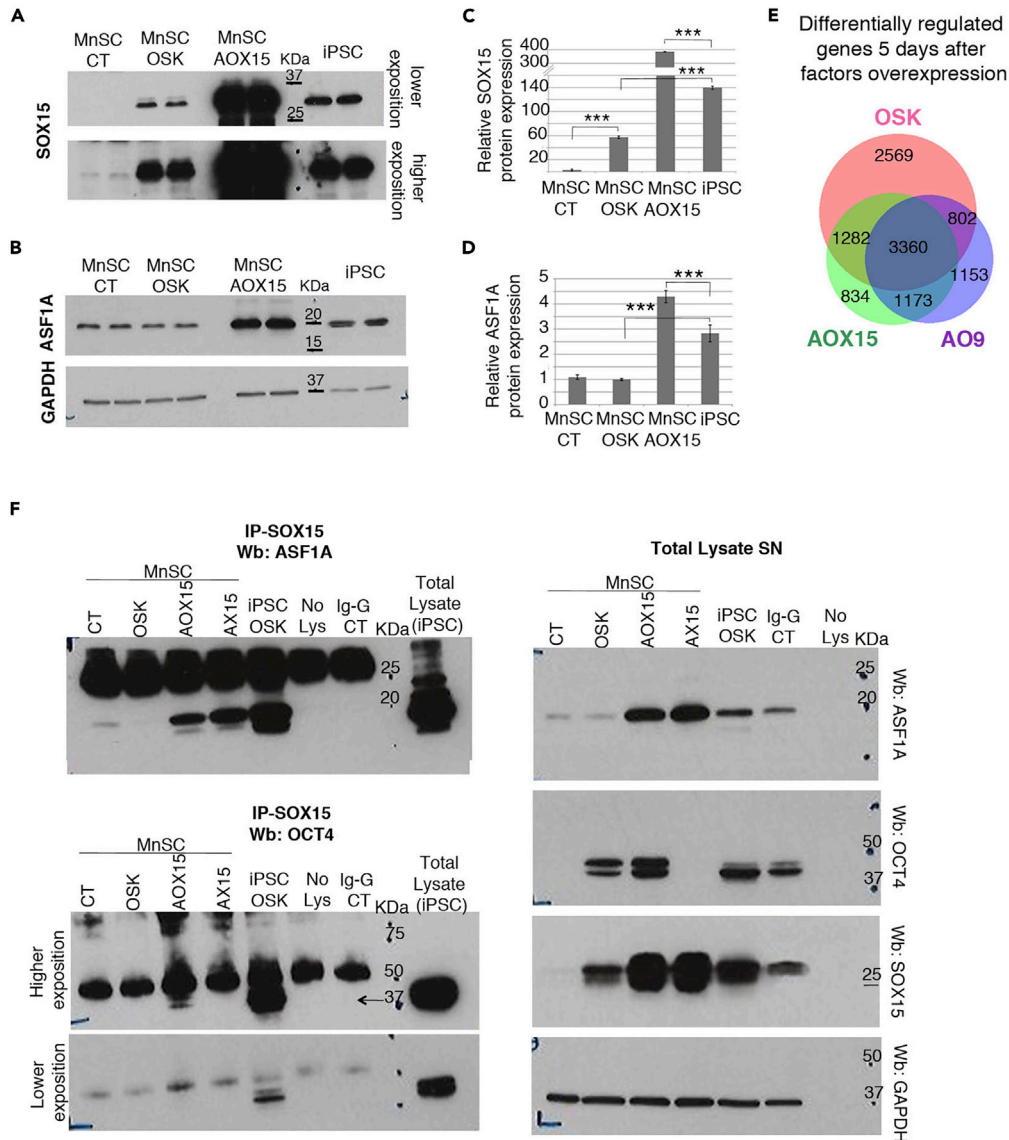
**Figure 3. Reprogramming Occurs Through Different Mechanisms and Pathways Depending on Triggering Combination**

(A–D) SOX15 is upregulated early during reprogramming. MnSCs lysates 5 days after retroviral driven overexpression of GFP (MnSC CT), OSK (MnSC-OSK), or AOX15 (MnSC-AOX15) and OSK-iPSCs were used for western blot against SOX15 (A) and ASF1A (B) and loading control GAPDH. (C and D) Quantification of band pixel intensity relative to GAPDH was done. Data correspond to the average of three independent experiments (three different MnSCs donors) done in duplicate (mean values ± SEM). Student's t test was applied for statistical significance: ***p < 0.001.

(E) Proportional Venn diagram showing differentially regulated genes 5 days after OSK, AOX15, or AO9 reprogramming factors overexpression using array-based global gene expression analysis. MnSCs overexpressing GFP were used as control (CT).

(F) SOX15 protein interaction during reprogramming and pluripotency. MnSCs lysates 5 days after retroviral driven overexpression of GFP, OSK, AOX15, or AX15 and fully reprogrammed OSK-iPSCs were used for SOX15 immunoprecipitation (IP) and western blot (Wb) against ASF1A and OCT4. Cell lysate supernatants (SN) were recovered after IP and use for western blot (right panels).

See also Figure S2.

We further investigated whether SOX15 participates in ASF1A-OCT4 reprogramming through interaction with this protein complex (Gonzalez-Munoz et al., 2014).

We found that, although SOX15 protein interacts with both ASF1A and OCT4 in pluripotent iPS cells, during reprogramming initiation, SOX15 only interacts with OCT4 when we use AOX15, but not OSK, combination (Figure 3F).

Similarly, protein interaction between ASF1A and SOX15 is observed not only during AOX15 and not during OSK reprogramming but also when both proteins, ASF1A and SOX15, are overexpressed indicating this interaction is OCT4 independent.

Interestingly, even if at lower degree, we saw ASF1A-SOX15 interaction also in control MnSCs, suggesting a possible hypothesis that MnSCs higher reprogramming capacity may be associated with a basal oocyte-related switched-on state.

Our results show that direct interaction of SOX15 with both ASF1A and OCT4 is part of the specific mechanism of the AOX15 combination and leads to distinct initiation pathways for reprogramming that include later MET activation.

## AOX15 Reprogrammed iPSCs Show Distinguishable Pluripotent State

We next characterized the pluripotent cells generated. AOX15-derived colonies were fully reprogrammed, expressing standard stem cell markers after culturing for 25–28 passages (Figures 4A, 4B, and S3A) and showed normal karyotype (Figure S3B). We found no detectable expression of exogenous factors from the retroviral vectors (Figure S3C). When induced to differentiate *in vitro*, OSK-iPSCs and AOX15-iPSCs can form ecto-, endo-, and mesoderm cell lineages (Figures S4A and S4B) and formed mature teratomas when injected into immunodeficient mice (Figure S4C).

We performed whole-transcriptome profiling on our cohort of genetically matched OSK and AOX15 hiPSCs. hESCs were used as control to confirm the pluripotent expression profile of hiPSCs generated (Figure 4C). Although, as expected, there are strong overlaps among all three pluripotent groups, supporting achieved full reprogramming of iPSCs, AOX15-iPSCs specifically regulate the expression of ~13% of the genes compared with OSK-iPSCs (Figure 4C) (Table S3). Their GO analysis revealed a significant enrichment for biological processes where we found a number of genes that are also either highly expressed or have an essential functional role in human MII oocytes (Table S4).

Whole-genome CpG DNA methylation analysis confirmed expected hypermethylation (Nishino et al., 2011) of all pluripotent groups compared with MnSC cells (Figure 4D). Unsupervised hierarchical clustering and PCA of whole-genome CpG DNA methylation data revealed separated clustering of OSK from AOX15 hiPSCs (from same MnSCs donors) as well as from hESCs (Figures 4E and 4F), and we can identify specific differentially methylated regions (DMRs) for each of the reprogramming combinations (Figure 4G and Table S3).

Together, these results further support that differential pathways to reach pluripotency, depending on triggering combination factors, leads to a distinguishable pluripotent state.

## Superior Differentiation Potential of AOX15-iPSCs

We hypothesized differences found in OSK and AOX15-iPSCs have a functional effect on their differentiation capacity.

We assessed the potential of pluripotent lines to spontaneously differentiate *in vitro* and quantified trilineage potential using ScoreCard assays (Bock et al., 2011) at two time points (10 and 21 days). We analyzed the expression plots of 94 genes, relative to the undifferentiated reference set (Figures 5A and 5C). Although, as expected, the Scorecard analysis algorithm predicts trilineage potential for all cell lines, we found a significant higher trend for mesodermal and endodermal differentiation in AOX15-iPSCs compared with OSK-iPSCs, both at early and late stages, suggesting their highest differentiation potential (Figures 5B and 5D).
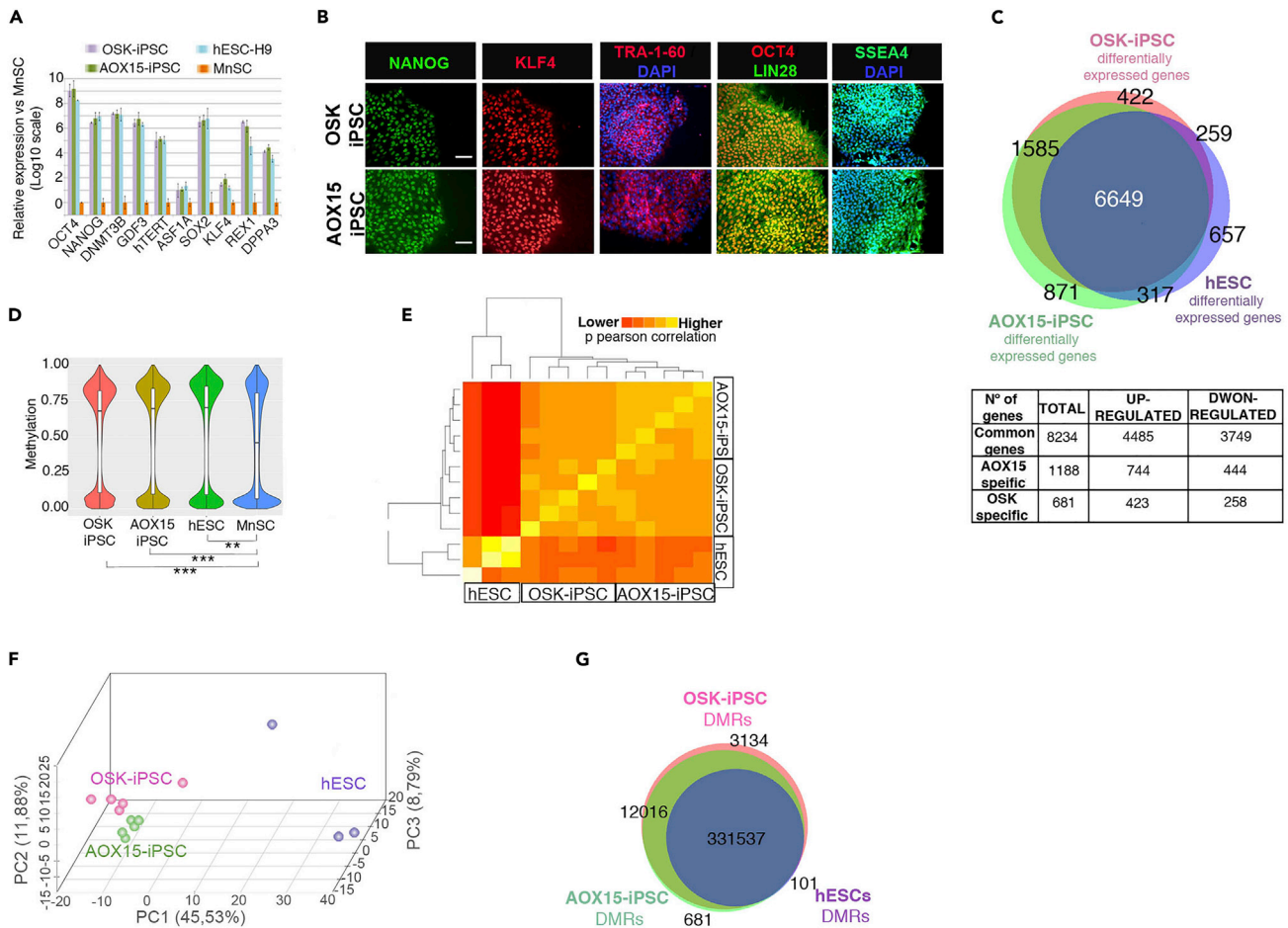
**Figure 4. AOX15 Reprogrammed iPSCs Show Distinguishable Pluripotent State**

(A) qRT-PCR for genes characteristic of pluripotent cells was performed as indicated on mRNA collected from source MnSCs and reprogrammed iPSC using OSK or AOX15 combination and H9-hESCs. Values indicate relative expression of the specific gene normalized to GAPDH/Actin relative to MnSC-GFP expression, which was arbitrarily assigned a value of 0, in a logarithmic scale. Data correspond to the average of three independent experiments done in triplicate (three different iPSC clones/MnSC cell line) (n = 9, mean values ± SEM) with cells from three different MnSC donors.

(B) Representative immunofluorescence analysis image of pluripotent markers on OSK and AOX15 iPSC colonies shows similar staining pattern (scale bar, 100 μm).

(C) High-throughput array-based expression analysis of MnSC derived OSK- and AOX15-iPSCs, and H9-hESCs. Differentially regulated genes after either reprogramming combination were used to generate Venn diagrams to identify specific and common regulated genes in each pluripotent group. Representative pluripotency-associated genes are shown.

(D) Violin plots showing the distribution of the DNA methylation (beta values) in each of the pluripotent group and MnSCs. Significant global methylation compared with MnSC is shown (p values: ***$p < 0.001$, **$<0.01$).

(E) Heatmap showing the clustering of MnSC derived OSK and AOX15 lines (five lines from four different MnSC donors each) and hESCs (H9 p33 and H9 p67, and H1) using the DNA methylation (array-based) data. Euclidean distance and complete agglomeration method were used to compute the heatmap's dendrogram. Correlation was computed with Pearson's method.

(F) PCA analysis using methylation data as in (E).

(G) High-throughput array-based DNA methylation analysis of MnSC derived OSK- and AOX15-iPSCs, and H9-hESCs. Differentially methylated regions (DMRs) after either reprogramming combination were used to generate Venn diagrams to identify specific and common methylated genomic regions in each pluripotent group.

See also Figures S3 and S4.

To prove the functional consequences of differential activation of lineage-specific transcription, we evaluated specific mesoderm and endoderm cell types *in vitro* for differentiation potential toward cardiomyocytes and pancreatic progenitor cells, respectively.
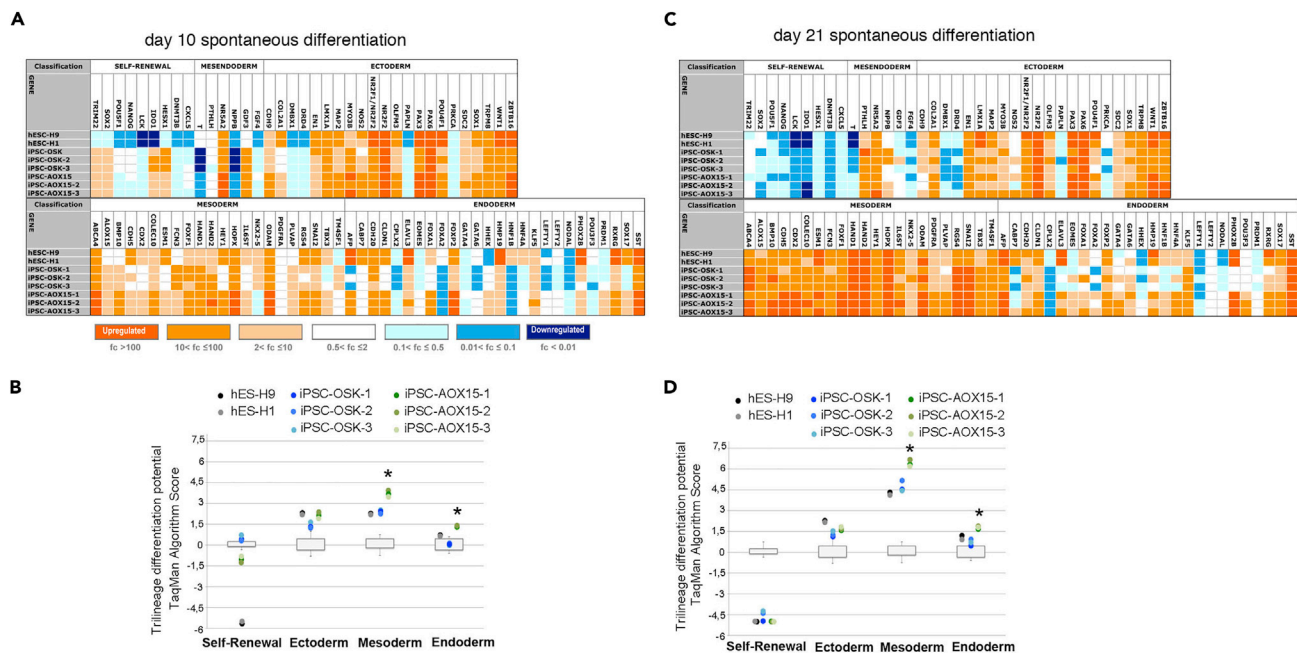
**Figure 5. AOX15 and OSK iPSCs Show Differential Spontaneous Differentiation Potential**

Embryo bodies were derived from hESCs (H9 and H1) or MnSC derived OSK and AOX15 iPSCs (three iPSC lines from three different donors/combination) at two time points of spontaneous *in vitro* differentiation. Heatmap expression (A and C) and dot blot scores (B and D) generated by the ScoreCard algorithm showing expression of pluripotency and differentiation markers at day 10 of floating EBs culture or after 11 more days (21 days) of attached EBs culture. *p < 0.05 one-way ANOVA with TUKEY post hoc test.

We examined the relative amount of cardiac troponin T-positive cells by immunofluorescence, flow cytometry, and relative gene expression of cardiac-specific markers (Figures 6A–6C). Our results confirmed the highest cardiac differentiation potential of AOX15-iPSCs.

Similarly, AOX15-iPSCs efficiently differentiate to PDX1-positive cells (Figures 6D and 6E) and show the highest pancreatic progenitor markers expression (Figure 6F).

We further assessed their capacity for primordial germ cells (PGC-like) specification as a number of reports have shown the low efficiency of this process using hiPSCs and the importance of the highly orchestrated combination of transcriptional and epigenetic state of the original cells (Canovas et al., 2017; Irie et al., 2015; Sasaki et al., 2015). We found iPSCs differentiate to VASA and PRMT5-positive cells (Figure 6G), and qPCR showed AOX15-iPSCs present significantly higher relative expression of PGC markers than OSK-iPSCs (Figure 6H). Together, our data support that AOX15-iPSCs have superior differentiation capacity.

## DISCUSSION

We provide compelling evidence of the importance of deep characterization of original somatic cells to provide crucial information involved in the reprogramming phenomenon.

We found MnSCs have unique expression and epigenetic and potency profiles and show higher reprogramming efficiency than hADFs and BM-MSCs. Although high reprogramming capacity has been shown previously for these cells (de Carvalho Rodrigues et al., 2012; Li et al., 2012), no rigorous comparative analysis has been made and, contrary to our data, high efficiency has been attributed to theoretical basal multipotent state, although marker analysis has been controversial and discordant among publications (de Carvalho Rodrigues et al., 2012; Khanjani et al., 2014; Li et al., 2012), probably due to an absence of appropriate controls.
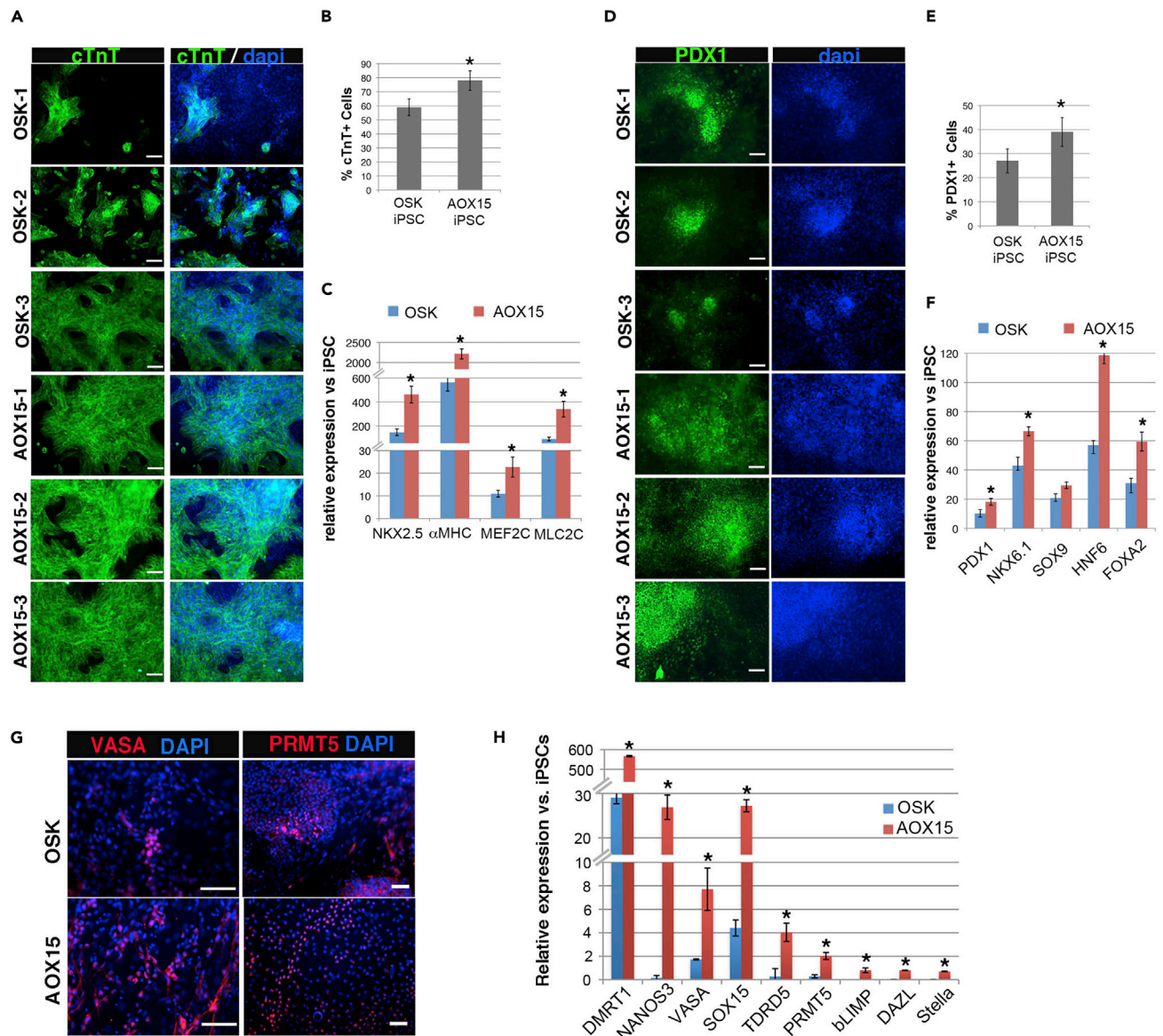
**Figure 6. AOX15-iPSCs Show Increased Cardiomyocyte, Pancreatic Progenitors, and Primordial Germ Cell (PGC) Differentiation Efficiency**

(A–C) Efficiency of *in vitro* differentiation toward cardiomyocytes of OSK- and AOX15-iPSCs 14 days after induction. (A) Immunocytochemistry analysis of cardiomyocyte cell marker Cardiac troponin T (cTnT). DAPI was used for nucleus labeling (scale bar, 80 μm). (B) Flow cytometric analysis at 14 days post induction of cardiac differentiation using OSK- or AOX15-iPSCs. Data are expressed as mean ± SEM (n = 9) with cells from three different donor-iPSCs. *p < 0.05 t test. (C) qRT-PCR data for cardiomyocyte differentiation markers NKX2.5, αMHC, MEF2C, MLC2C at day 14 of *in vitro* differentiation. Average expression values ±SEM are represented relative to undifferentiated iPSCs (normalized to GAPDH/Actin). Data correspond to the average of three independent experiments done in triplicate with cells from three different donor-iPSCs (n = 9). Student's t test was applied for statistical significance: *p < 0.05 between OSK and AOX15 groups.

(D–F) Efficiency of *in vitro* differentiation toward pancreatic progenitors of OSK- and AOX15-iPSCs generated after 15 days of differentiation using the STEMdiff directed differentiation kit. (D) Immunocytochemistry analysis of pancreatic progenitors marker PDX1 with cells from three different donor-iPSCs (scale bar, 80 μm). (E) Flow cytometric analysis at 15 days post induction of pancreatic progenitor differentiation using OSK- or AOX15-iPSCs. Data are expressed as mean ± SEM (n = 9) with cells from three different donor-iPSCs. *p < 0.05 t test. (F) qRT-PCR data for pancreatic progenitor differentiation markers PDX1, NKX6.1, SOX9, NGN3, HNF6, FOXA2. Average expression values ±SEM are represented relative to undifferentiated iPSCs (normalized to GAPDH/Actin). Data correspond to the average of three independent experiments done in triplicate with cells from three different donor-iPSCs (n = 9). Student's t test was applied for statistical significance: p*<0.05 between OSK and AOX15 groups.

(G and H) Efficiency of *in vitro* differentiation toward primordial germ cell (PGC) fate. (G) Immunocytochemistry images of PGC differentiation markers VASA and PRMT5 (scale bar, 60 μm). (H) qRT-PCR data for PGC differentiation markers. Average expression values ±SEM are represented relative to undifferentiated iPSCs (normalized to GAPDH/Actin). Data correspond to the average of three independent experiments done in triplicate with cells from three different donor-iPSCs (n = 9). Student's t test was applied for statistical significance: p*<0.05 between OSK and AOX15 groups.

Our analysis, focused on the oocyte-related signature of MnSCs, has uncovered SOX15 as a crucial human reprogramming factor. We found SOX15 expression is upregulated in human pluripotent cells, matching mouse ES data (Maruyama et al., 2005), and also during early reprogramming.

We show SOX15 overexpression, together with ASF1A and OCT4, creates an efficient "oocyte-based" reprogramming combination (AOX15) that follows a reprogramming mechanism different from the canonical OSK combinations.

Our co-immunoprecipitation assays show AOX15, but not OSK, reprogramming initiation functions by SOX15 interaction with both ASF1A and OCT4, generating specific early transcriptional activation program, and finally reaches a unique pluripotent state that has relevant functional consequences with increased differentiation potential, including challenging PGC-like generation.

Our work supports the hypothesis that pluripotency is not a single state—previous revolutionary publications in this field have shown the existence of naive and ground human iPSC and ESC, and the following research confirms the complexity of such definitions—and more progress is needed to explore the possibility of additional pluripotent states or, probably more accurately, sequences of pluripotency states, that can resemble the natural progression after fertilization.

Exogenous factor reprogramming through iPSCs constitutes an exceptional tool for such study allowing the analysis of specific triggering combinations as the one described here that will help uncover other crucial factors for pluripotency, reprogramming, and development. We believe the use of oocyte significant factors together with somatic cell nuclear transfer information will comprise a valuable source for this goal.

### Limitations of the Study

We have focused on analysis and characterization of AOX15 reprogramming with MnSCs; however, full characterization of the role of SOX15 in oocyte-based reprogramming in cell types of diverse origin would also bring valuable information of the reprogramming process. Our results indicate SOX15 oocyte-based reprogramming operates also in cell types of mesenchymal origin as hADFs and BM-MSCs, although at lower efficiency than MnSCs. Our hypothesis considers endogenous basal-activated pathways associated with oocyte-factors in somatic cells influence their reprogramming efficiency depending on the combination we choose; further studies are needed to decipher such basal-activated pathways and their relation with the ease for reprogramming.

Also, it would be interesting to provide deeper mechanistic insight into this process. A possible strategy would be to disrupt SOX15 interaction with ASF1A, OCT4, or both. Information of SOX15 and ASF1A interaction domains at protein level would be needed, and it is part of our future projects to perform biochemical and molecular characterization of ASF1A and SOX15 complex to uncover factors involved in reprogramming initiation.

### Resource Availability

#### Lead Contact

Further information and requests for resources and reagents should be directed to and will be fulfilled by the lead contact Elena Gonzalez-Munoz (egonmu@uma.es).

#### Materials Availability

All material used are listed in Transparent Methods section and Key Resources Table in Supplemental Information, and any further information and requests for resources and reagents should be directed to and will be fulfilled by the Lead Contact.

#### Data and Code Availability

The accession number for the expression and methylation arrays data reported in this paper is NCBI's Gene Expression Omnibus (GEO) repository: GSE139085 (https://www.ncbi.nlm.nih.gov/geo/query/acc.cgi?acc=GSE139085).

## AUTHOR CONTRIBUTIONS

Funding acquisition: E.G.-M. Conceived and designed experiments: E.G.-M. Performed experiments: E.G.-M., L.L.-C. Analyzed the data: E.G.-M. Bioinformatic analysis: J.M.-M., P.C.-S. Wrote the manuscript: E.G.-M.

## DECLARATION OF INTERESTS

The authors declare no competing interests.

## REFERENCES

Assou, S., Anahory, T., Pantesco, V., Le Carrour, T., Pellestor, F., Klein, B., Reyftmann, L., Dechaud, H., De Vos, J., and Hamamah, S. (2006). The human cumulus–oocyte complex gene-expression profile. Hum. Reprod. 21, 1705–1719.

Assou, S., Cerecedo, D., Tondeur, S., Pantesco, V., Hovatta, O., Klein, B., Hamamah, S., and De Vos, J. (2009). A gene expression signature shared by human mature oocytes and embryonic stem cells. BMC Genomics 10, 10.

Awe, J.P., and Byrne, J.A. (2013). Identifying candidate oocyte reprogramming factors using cross-species global transcriptional analysis. Cell Reprogram 15, 126–133.

Bock, C., Kiskinis, E., Verstappen, G., Gu, H., Boulting, G., Smith, Z.D., Ziller, M., Croft, G.F., Amoroso, M.W., Oakley, D.H., et al. (2011). Reference Maps of human ES and iPS cell variation enable high-throughput characterization of pluripotent cell lines. Cell 144, 439–452.

Buganim, Y., Faddah, D.A., and Jaenisch, R. (2013). Mechanisms and models of somatic cell reprogramming. Nat. Rev. Genet. 14, 427–439.

Canovas, S., Campos, R., Aguilar, E., and Cibelli, J.B. (2017). Progress towards human primordial germ cell specification in vitro. Mol. Hum. Reprod. 23, 4–15.

de Carvalho Rodrigues, D., Asensi, K.D., Vairo, L., Azevedo-Pereira, R.L., Silva, R., Rondinelli, E., Goldenberg, R.C., Campos de Carvalho, A.C., and Urmenyi, T.P. (2012). Human menstrual blood-derived mesenchymal cells as a cell source of rapid and efficient nuclear reprogramming. Cell Transplant 21, 2215–2224.

Gonzalez-Munoz, E., Arboleda-Estudillo, Y., Otu, H.H., and Cibelli, J.B. (2014). Cell reprogramming. Histone chaperone ASF1A is required for maintenance of pluripotency and cellular reprogramming. Science 345, 822–825.

Gonzalez-Munoz, E., and Cibelli, J.B. (2018). Somatic cell reprogramming informed by the oocyte. Stem Cells Dev. 27, 871–887.

Irie, N., Weinberger, L., Tang, W.W., Kobayashi, T., Viukov, S., Manor, Y.S., Dietmann, S., Hanna, J.H., and Surani, M.A. (2015). SOX17 is a critical specifier of human primordial germ cell fate. Cell 160, 253–268.

Jullien, J., Miyamoto, K., Pasque, V., Allen, G.E., Bradshaw, C.R., Garrett, N.J., Halley-Stott, R.P., Kimura, H., Ohsumi, K., and Gurdon, J.B. (2014). Hierarchical molecular events driven by oocyte-specific factors lead to rapid and extensive reprogramming. Mol. Cell 55, 524–536.

Khanjani, S., Khanmohammadi, M., Zarnani, A.H., Akhondi, M.M., Ahani, A., Ghaempanah, Z., Naderi, M.M., Eghtesad, S., and Kazemnejad, S. (2014). Comparative evaluation of differentiation potential of menstrual blood- versus bone marrow-derived stem cells into hepatocyte-like cells. PLoS One 9, e86075.

Kocabas, A.M., Crosby, J., Ross, P.J., Otu, H.H., Beyhan, Z., Can, H., Tam, W.L., Rosa, G.J., Halgren, R.G., Lim, B., et al. (2006). The transcriptome of human oocytes. Proc. Natl. Acad. Sci. U S A 103, 14027–14032.

Lee, H.J., Goring, W., Ochs, M., Muhlfeld, C., Steding, G., Paprotta, I., Engel, W., and Adham, I.M. (2004). Sox15 is required for skeletal muscle regeneration. Mol. Cell. Biol. 24, 8428–8436.

Li, R., Liang, J., Ni, S., Zhou, T., Qing, X., Li, H., He, W., Chen, J., Li, F., Zhuang, Q., et al. (2010). A mesenchymal-to-epithelial transition initiates and

is required for the nuclear reprogramming of mouse fibroblasts. Cell Stem Cell 7, 51–63.

Li, Y., Li, X., Zhao, H., Feng, R., Zhang, X., Tai, D., An, G., Wen, J., and Tan, J. (2012). Efficient induction of pluripotent stem cells from menstrual blood. Stem Cells Dev. 22, 1147–1158.

Maruyama, M., Ichisaka, T., Nakagawa, M., and Yamanaka, S. (2005). Differential roles for Sox15 and Sox2 in transcriptional control in mouse embryonic stem cells. J. Biol. Chem. 280, 24371–24379.

Meeson, A.P., Shi, X., Alexander, M.S., Williams, R.S., Allen, R.E., Jiang, N., Adham, I.M., Goetsch, S.C., Hammer, R.E., and Garry, D.J. (2007). Sox15 and Fhl3 transcriptionally coactivate Foxk1 and regulate myogenic progenitor cells. EMBO J. 26, 1902–1912.

Mi, H., Muruganujan, A., Ebert, D., Huang, X., and Thomas, P.D. (2019). PANTHER version 14: more genomes, a new PANTHER GO-slim and improvements in enrichment analysis tools. Nucleic. Acids Res. 47, D419–D426.

Nakagawa, M., Koyanagi, M., Tanabe, K., Takahashi, K., Ichisaka, T., Aoi, T., Okita, K., Mochiduki, Y., Takizawa, N., and Yamanaka, S. (2008). Generation of induced pluripotent stem cells without Myc from mouse and human fibroblasts. Nat. Biotechnol. 26, 101–106.

Ng, C.K., Li, N.X., Chee, S., Prabhakar, S., Kolatkar, P.R., and Jauch, R. (2012). Deciphering the Sox-Oct partner code by quantitative cooperativity measurements. Nucleic Acids Res. 40, 4933–4941.

Nishino, T., Kanata, S., and Umezawa, Y. (2011). Selective visualization of point defects in carbon nanotubes at the atomic scale by an electron-donating molecular tip. Chem. Commun. (Camb.) 47, 7467–7469.

Ohnishi, H., Oda, Y., Aoki, T., Tadokoro, M., Katsube, Y., Ohgushi, H., Hattori, K., and Yuba, S. (2011). A comparative study of induced pluripotent stem cells generated from frozen, stocked bone marrow- and adipose tissue-derived mesenchymal stem cells. J. Tissue Eng. Regen. Med. 6, 261–271.

Pacini, S., Carnicelli, V., Trombi, L., Montali, M., Fazzi, R., Lazzarini, E., Giannotti, S., and Petrini, M. (2010). Constitutive expression of pluripotency-associated genes in mesodermal progenitor cells (MPCs). PLoS One 5, e9861.

Park, I.H., Arora, N., Huo, H., Maherali, N., Ahfeldt, T., Shimamura, A., Lensch, M.W., Cowan, C., Hochedlinger, K., and Daley, G.Q. (2008). Disease-specific induced pluripotent stem cells. Cell 134, 877–886.

Patel, M., and Yang, S. (2010). Advances in reprogramming somatic cells to induced pluripotent stem cells. Stem Cell Rev. 6, 367–380.

Sasaki, K., Yokobayashi, S., Nakamura, T., Okamoto, I., Yabuta, Y., Kurimoto, K., Ohta, H., Moritoki, Y., Iwatani, C., Tsuchiya, H., et al. (2015). Robust in vitro induction of human germ cell fate from pluripotent stem cells. Cell Stem Cell 17, 178–194.

Shao, K., Koch, C., Gupta, M.K., Lin, Q., Lenz, M., Laufs, S., Denecke, B., Schmidt, M., Linke, M., Hennies, H.C., et al. (2012). Induced pluripotent mesenchymal stromal cell clones retain donor-derived differences in DNA methylation profiles. Mol. Ther. 21, 240–250.

Streckfuss-Bomeke, K., Wolf, F., Azizian, A., Stauske, M., Tiburcy, M., Wagner, S., Hubscher, D., Dressel, R., Chen, S., Jende, J., et al. (2012). Comparative study of human-induced pluripotent stem cells derived from bone marrow cells, hair keratinocytes, and skin fibroblasts. Eur. Heart J. 34, 2618–2629.

Subramanyam, D., Lamouille, S., Judson, R.L., Liu, J.Y., Bucay, N., Derynck, R., and Blelloch, R. (2011). Multiple targets of miR-302 and miR-372 promote reprogramming of human fibroblasts to induced pluripotent stem cells. Nat. Biotechnol. 29, 443–448.

Yoshikawa, T., Piao, Y., Zhong, J., Matoba, R., Carter, M.G., Wang, Y., Goldberg, I., and Ko, M.S. (2006). High-throughput screen for genes predominantly expressed in the ICM of mouse blastocysts by whole mount in situ hybridization. Gene Expr. Patterns 6, 213–224.

**Supplemental Information**

# Analysis of Menstrual Blood Stromal Cells

# Reveals SOX15 Triggers Oocyte-Based

# Human Cell Reprogramming

Lidia Lopez-Caraballo, Jordi Martorell-Marugan, Pedro Carmona-Saez, and Elena Gonzalez-Muñoz
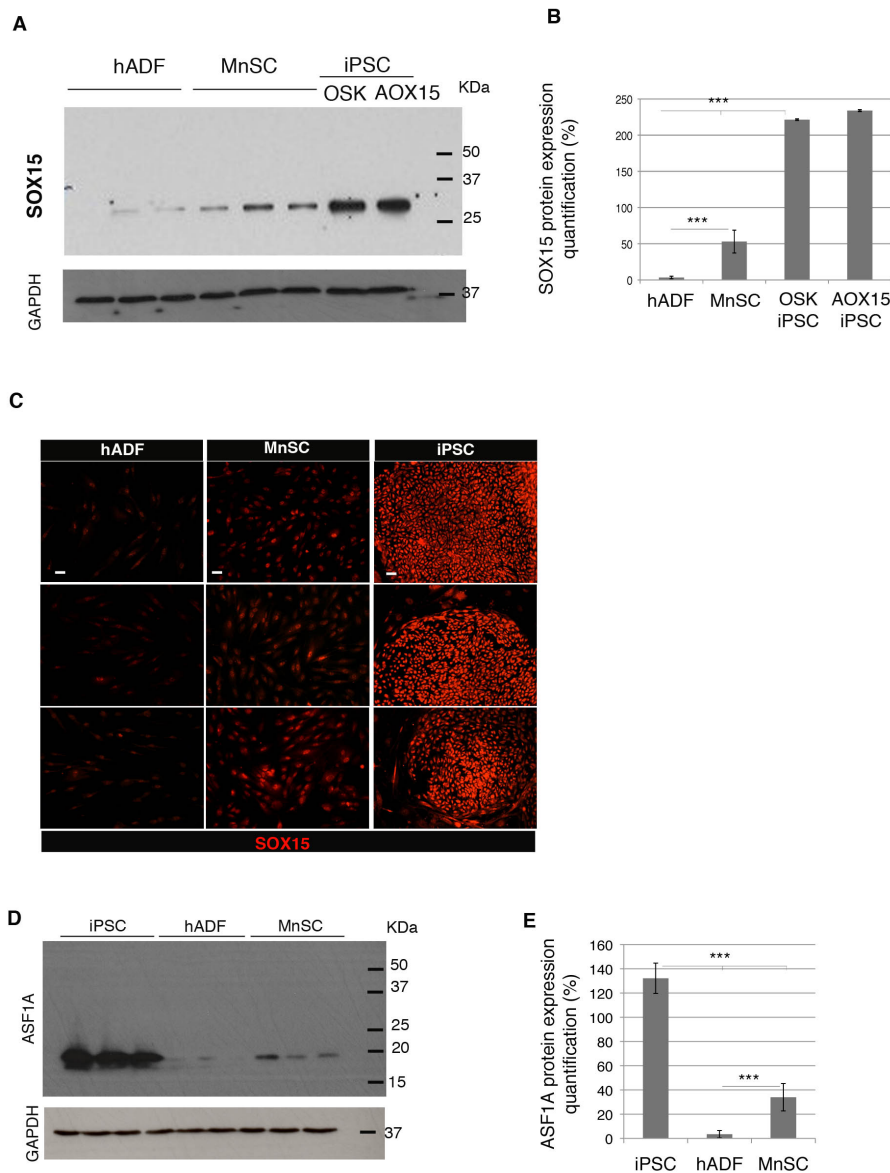
**Figure S1. MnSCs present higher amount of the oocyte-enriched proteins ASF1A and SOX15 than hADFs**. Related to Figure 1.

A. hADF, MnSC and AOX15OSK-iPSCs from same three different donors were lysed, total protein SDS-PAGE and western blot against SOX15 (A) and ASF1A (D) and loading control GAPDH was performed. B. Quantification of band pixel intensity relative to GAPDH, showed significant increment on SOX15 (B) and ASF1A (E) presence in MnSC over hADF with iPSC showing the highest expression. Data correspond to the average of 3 independent experiments (three different MnSCs and hADFs) done in duplicate (***P<0.001 T-Test significance value).

C. Immunocytochemistry analysis of SOX15 expression on MnSC, hADFs and OSK-iPSCs from three different donors showing different intensities of SOX15 nuclear staining. Representative fluorescence microscopy images using identical exposition time for all cell types (Scale bar= 30 µm).

**A**



**B**



d10 after transduction

**C**



d18 after transduction
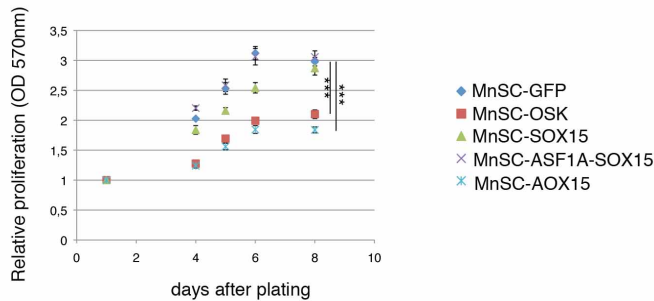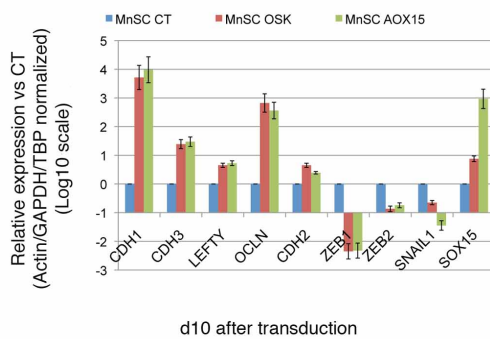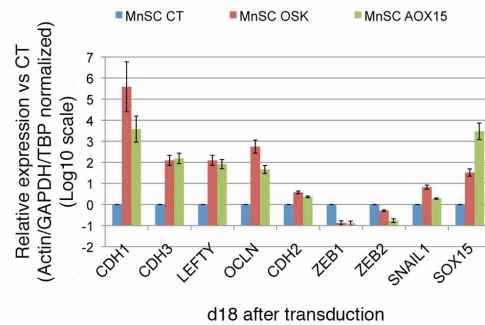
**Figure S2**. **Early effect of OSK and AOX15 overexpression on MnSC**. Related to Figure 3.
A. OSK and AOX15 reprogramming factors overexpression reduces MnSCs proliferation rate. Two days after specific factor combination overexpression, 25.000 MnSCs were plated for proliferation/viability MTT assay. Cells were recovered 1, 4, 5, 6 and 8 days after, to measure 570nm absorbance reflecting number of viable cells (MTT assay). Average relative absorbance ± SEM (relative to day 1) are represented. Data correspond to the average of 3 independent experiments (three different MnSCs) done in duplicate, ***P>0.001, **>0.05, *>0.01 T-Test significance value compared to MnSC-GFP
B,C. Expression of markers for MET/cell adhesion during reprogramming. MnSCs where transduced using specified factors combination and seeded into MEF cells for reprogramming. 10 days (B) and 18 days (C) after transduction total mRNA was used for qRT-PCR analysis of MET markers (CDH1, CDH3, LEFTY, OCLN), EMT markers (CDH2, ZEB1, ZEB2 and SNAIL1) and SOX15 expression. Mean values (n=3 from different donors) ± SEM are plotted indicating expression of the specific gene normalized to GAPDH/Actin relative to MnSC-GFP expression at the specified time point, which was arbitrarily assigned a value of 0, in a logarithmic scale.
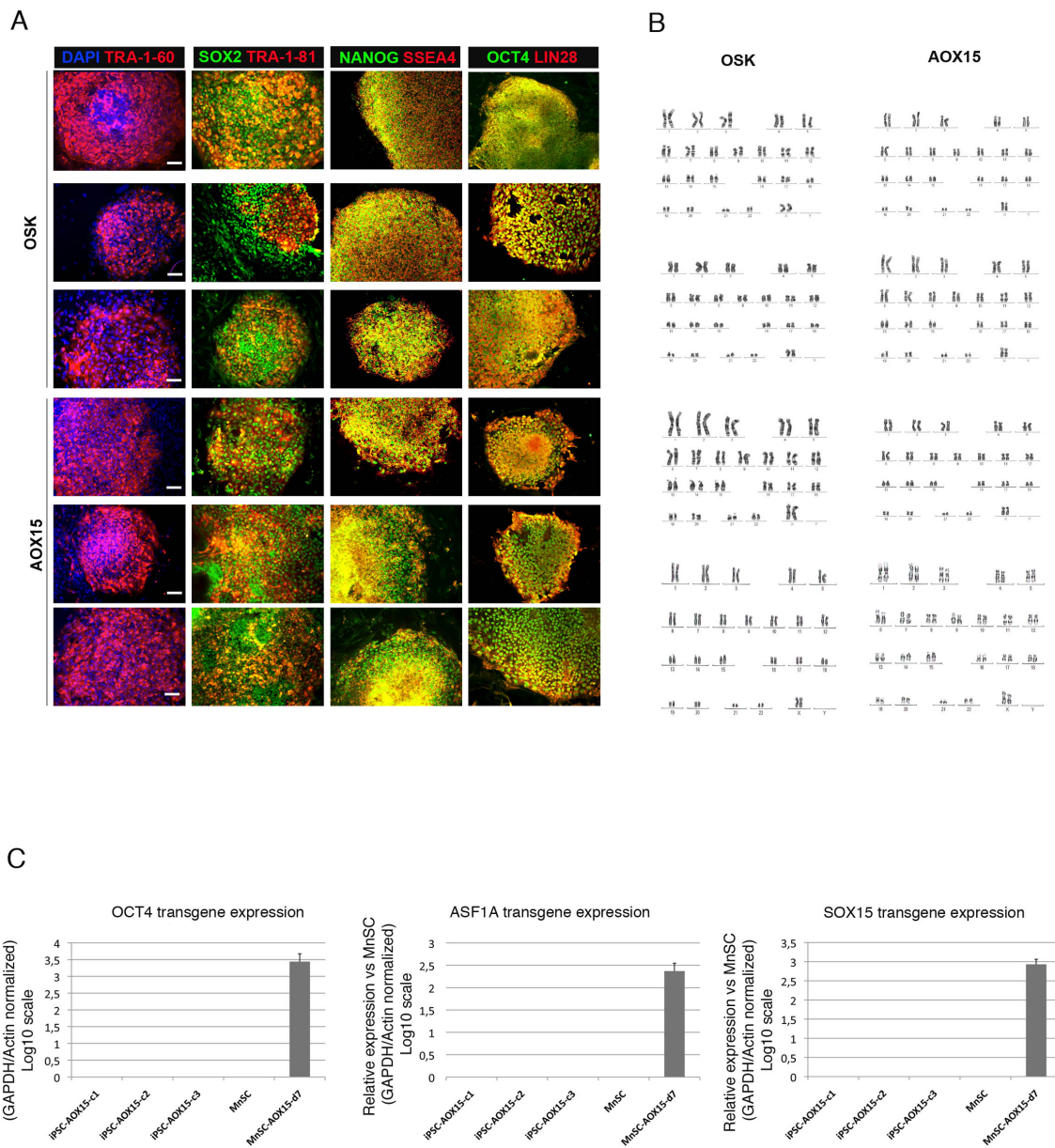
**Figure S3**. **iPSC lines pluripotency characterization**. Related to Figure 4.
Representative immunofluorescence image of pluripotent markers on OSK and AOX15 iPSC colonies derived from three different MnSC donors shows similar staining pattern (Scale bar= 100 μm). B. High-resolution G-banded karyotypes. Representative four clones of fully reprogrammed OSK and AOX15 iPSCs from MnSCs from four different donors showing normal karyotype. C. Transgen silencing after AOX15 reprogramming. Quantitative PCR for expression of retroviral transgenes in three AOX15-iPS cell lines, MnSCs control, and MnSCs 7 days after the transduction with the three retroviral vectors (hADF-AOX15-7d). Mean values (n=3) ± SEM are plotted indicating expression of the specific gene normalized to GAPDH/Actin relative to MnSC expression, which was arbitrarily assigned a value of 0, in a logarithmic scale.

**A**



**B**



**C**
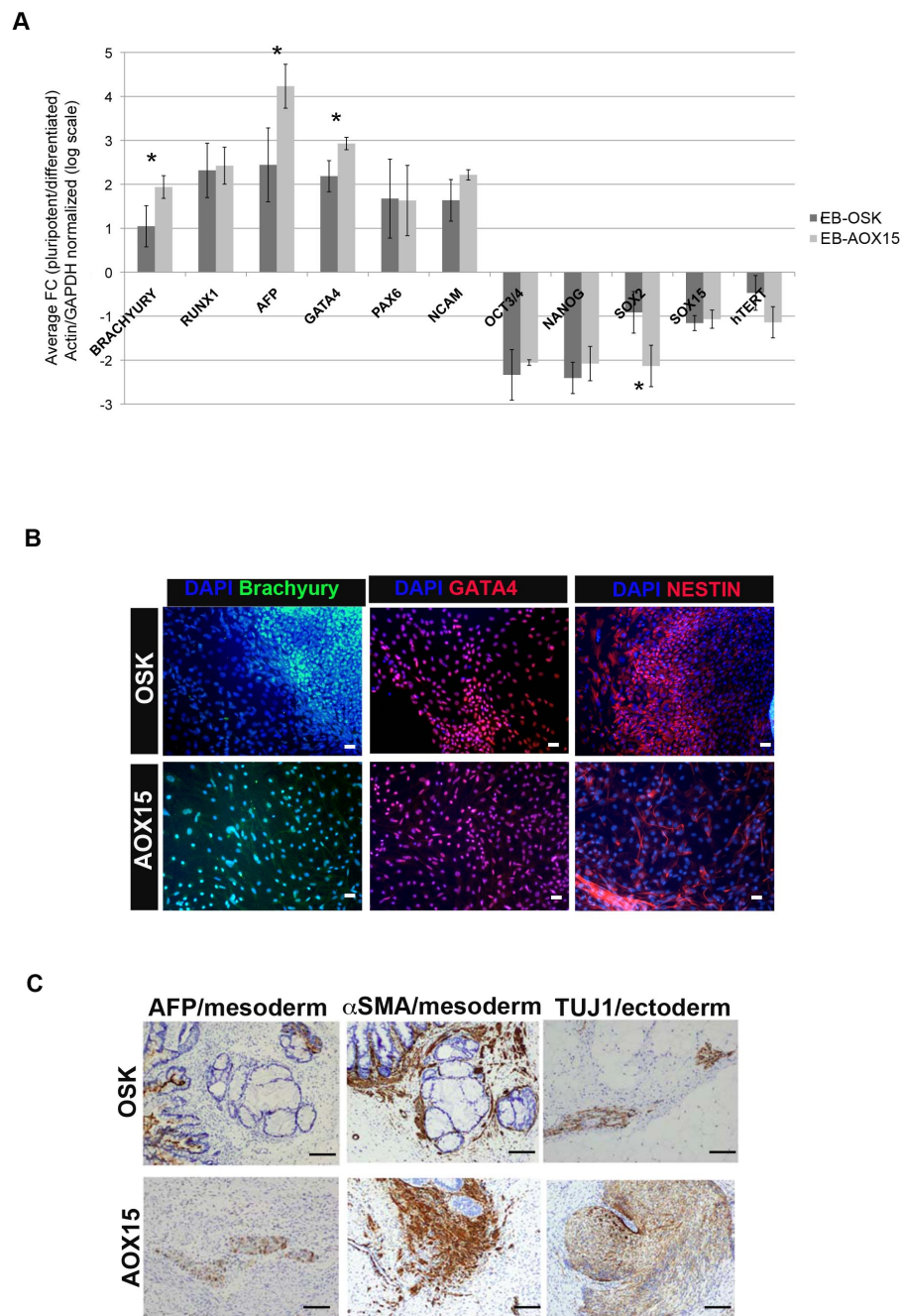


**Figure S4**. **iPSC characterization: in vitro and in vivo differentiation capacity**. Related to Figure 4.

A. qRT-PCR data showing uprelugation of differentiation markers GATA4 and AFP (endoderm), RUNX1 and BRACHURY (Mesoderm) and NCAM and PAX6 (ectoderm), and downregulation of pluripotency markers (OCT3/4, NANOG, SOX2 AND HTERT) and SOX15 at day10 of in vitro spontaneous differentiation protocol. Embryo bodies (EB) were derived from

OSK and AOX15 iPSCs. Average folding change expression values ± SEM (relative to undifferentiated iPSCs) are represented (logarithmic scale).

B. Representative image of immunocytochemistry analysis of specific markers of mesoderm (Brachyury), endoderm (GATA4), and ectoderm (Nestin) differentiation after spontaneous differentiation of each iPSC line (Scale bar= 30 μm).

C. Inmunohistochemistry of specific embryonic layers lineage markers on hematoxylin and eosin stained sections of representative matured OSK- and AOX15-iPS-derived teratomas exhibiting characteristic structure of intestinal epithelium (endoderm), cartilage (mesoderm) and neural epithelium (ectoderm)(Scale bar= 100 μm).

**TRANSPARENT METHODS**

**Experimental Model and Subject**

Cell Culture

H9 and H1 human ES (from Wiicell) and generated iPS cells were cultured in standard human ES cell culture medium (DMEM/F12 containing 20%KSR, 10ng/ml of human recombinant basic fibroblast growth factor (bFGF), 1xNEAA, 1xL-Glutamine, 5.5mM 2-ME, penicillin and streptomycin. ES cells and iPS cells were cultured on top of mitomycin-C mouse fibroblasts and picked mechanically as previously described (Gonzalez-Munoz et al., 2014). All cell lines were regularly tested for mycoplasma using PCR validation (Venor GeM Classic, Minerva Biolabs) and found to be negative.

Derivation of human adult somatic samples:

All samples were collected and processed after obtaining donors informed consent and with clearances from Stem cell ethical committee and Review Board of the National Research Ethics Service (PR-03-2018). All cultures were maintained at 37°C in a humidified atmosphere containing 5% CO2. All experiments were performed in passage 2-4. The specific protocol isolation for each cell type used is described below:

• Dermal fibroblasts (hADF) from biopsy samples: Primary skin fibroblasts were obtained via a 4-mm full-thickness skin punch biopsy from the surface of the upperback of the healthy volunteers. Cultured outgrowths appeared after 7–14 days. hADF were culture in DMEM containing 10%FBS, 1xNEAA, 1xL-Glutamine, penicillin and streptomycin (Byrne et al., 2009).

• hBM-MSCs were obtained from bone marrow of healthy volunteers according to published protocols (Casado-Diaz et al., 2008). Briefly, human bone marrow (BM) was aspirated from the iliac crest of healthy donors. Mononuclear cells were separated using the Ficoll hypaque (Sigma) gradient method. The cells were seeded at a density of $15 \times 10^4/cm^2$ in alpha-minimum essential medium (α-MEM) supplemented with 2 mM L-glutamine, 15% fetal bovine serum (FBS) (BioWhittaker, Switzerland), 100 U/ml Penicillin, 0.1 mg/ml Streptomycin Streptomycin and 1 ng/ml of fibroblast growth factor-basic (FGF-b, Peprotech EC, London,

UK). Cells were allowed to adhere for 48 h and non-adherent cells were washed out with phosphate-buffer saline (PBS) 100 mM pH 7,4 (Sigma-Aldrich, St Louis, MO). After 48 h, α-MEM supplemented with 10% FBS and 1 ng/ml FGF-b was added twice weekly. All cultures were maintained at 37°C in a humidified atmosphere containing 5% $CO_2$.

• MnSCs were obtained from menstrual blood of healthy volunteers at the peak of flow. Cells were centrifuged and submitted to the Ficoll (Histopaque 1077-Sigma) gradient according to the manufacturer's instructions. Mononuclear cells were culture in DMEM-F12 containing 10%FBS, 1xNEAA, 1xL-Glutamine, penicillin and streptomycin (Byrne et al., 2009).
All cell lines were regularly tested for mycoplasma using PCR validation (Venor GeM Classic, Minerva Biolabs) and found to be negative.

**Method Details**

Vectors

The cDNAs encoding hSOX15 (purchased from Open Biosystems) were subcloned into self-inactivating retroviral bicistronic vector pMX-GFP (Cell Biolabs, INC) using NotI and EcoRI restriction sites. DNA vectors pMX-GFP, pMX-OCT4, pMX-SOX2, pMX-KLF4 and pMX-cMYC (h.sapiens) were purchased from Addgene and pMX-ASF1A vector has been previously described by our group (Gonzalez-Munoz et al., 2014).

Cell Culture

H9 and H1 human ES (from Wiicell) and generated iPS cells were cultured in standard human ES cell culture medium (DMEM/F12 containing 20%KSR, 10ng/ml of human recombinant basic fibroblast growth factor (bFGF), 1xNEAA, 1xL-Glutamine, 5.5mM 2-ME, penicillin and streptomycin. ES cells and iPS cells were cultured on top of mitomycin-C mouse fibroblasts and picked mechanically as previously described (Gonzalez-Munoz et al., 2014). All cell lines were regularly tested for mycoplasma using PCR validation (Venor GeM Classic, Minerva Biolabs) and found to be negative.

Production of viral supernatants

For retrovectors, Hek293T cells were plated at 90% cell confluence in 10-cm dish. The next day, cells were transfected with 10μg viral vector, 7μg Gag-Pol vector (Addgene) and 3μg VSV-G plasmid (Addgene) using polyethylenimine method. Supernatant was collected 24 h and 48 h post-transfection and filtered through 45-mm pore size filters. Tittering was performed on Hek293Ts. 5 ml of unconcentrated viral supernatant was used to transduce 25,000 cells in the presence of 4μg/ml polybrene.

Reprogramming Assays

Low passage (passage 2-4) hADFs, BM-MSCs and MnSCs were seeded at 100.000 cells/well and transduced with retroviral supernatants encoding OSKM factors (pMX-OCT4, pMX-Sox2, pMX-KLF4 and pMX-cMYC), OSK or AOX15 (pMX-OCT4, pMX-ASF1A, pMX-SOX15) in the presence of 4 μg/ml polybrene. 24 hours later cells were replated onto six-well plates on a feeder layer of mitomycinC-treated mouse embryonic fibroblasts (Millipore). Medium was changed to hES medium daily. Colonies appear at day 18-28 after transduction. TRA-160+ iPSC colonies where individually picked and expanded for at least 5 passages before the iPS lines were confirmed positive for, Tra-1–60, SSEA-4 and NANOG by immunofluorescence. In all fully reprogrammed iPSCs vector-encoded transgenes were found to be silenced. For AO9 and AOX15-GDF9 iPSC generation we followed previously published protocol using 500nM GDF9 (Gonzalez-Munoz et al., 2014).

In vitro differentiation

     • For hADF, MnSC and BM-MSC differentiation to adipogenic, osteogenic and chondrogenic fate we used Human Mesenchymal Stem Cell Functional Identification Kit (RnDsystems) according to the manufacturer's instructions for 21 days. Neural differentiation was induced as described elsewhere (Delcroix et al., 2010; Hermann et al., 2006; Long et al., 2005). Briefly cells were cultured in KnockOutTM DMEM/F-12 Basal Medium (Invitrogen, San Diego, CA) supplemented with 20 ng/ml human epidermal growth factor (EGF, Peprotech, London, UK), 20 ng/ml bFGF, StemPro NSC SFM Supplement (1: 50; Invitrogen, San Diego, CA), and GlutaMAXTM-I Supplement (1:100; Invitrogen) at 37 C with 5 %$CO_2$, for 7-10 days.

• Pluripotent cells spontaneous differentiation was induced as previously described [13] by culturing ES cells as EBs in low attachment plates with hES media in the absence of bFGF during 7 days. EBs were transferred to 0.1% gelatin-coated dishes and cultured in differentiation medium (KO DMEM supplemented with 10% fetal bovine serum, 1x MEM nonessential amino acids, 2mML-glutamine, and 50uM-mercaptoethanol) up to 7 days. For the generation of neural precursors from pluripotent cells we followed our previous published protocol (Chang et al., 2010).

• iPSCs differentiation into pancreatic progenitors and into cardiomyocytes was done using the STEMdiff Pancreatic Progenitor kit and the the STEMdiff™ Cardiomyocyte Differentiation Kit (STEMCELL Technologies) respectively, according to the manufacturer's instructions. Tissue culture was carried out in 5% CO2 at 37°C.

• For PGC differentiation, we used validated protocol (Kee et al., 2009; Leng et al., 2015)with slight modifications. Briefly, iPS cells were detached from the feeder layers and suspended for 24 h in hES medium without bFGF to form embryoid bodies (EB). For primordial germ cells (PGCs) differentiation, EBs were initially cultured in DFSR (DMEM/F12 supplemented with 15% (v/v) knockout serum replacer medium 2 mM l-glutamine, 2 mM nonessential amino acids, 0.1 mM β-mercaptoethanol) containing 30 ng/ml Wnt3a (2324-WN; R&D, Minneapolis, MN, USA) for 24 h, and then the medium was changed to hES medium supplemented with 100 ng/ml bone morphogenetic protein 4 (BMP4, 314-BP; R&D, Minneapolis, MN, USA) for another 24 h. Subsequently, the EBs were plated on Matrigel-coated 6-well plates and cultured in DFSR medium containing 100 ng/ml BMP4. The medium was replaced every other day in the subsequent 14-day differentiation.

Animals

For teratoma analysis, NOD-SCID immunodeficient mice had been transferred from the Jackson Laboratories and housed and bred under the care of the animal house of *Biobanco del Sistema Publico Andaluz (BSSPA)*. Subcutaneous injection of iPS cells was performed under the ethical guidelines of Bionand committe according to protocols approved by Andalusian Regional Animal Research Committee. After four weeks, tumors were sectioned and processed for histological analysis (haematoxylin and eosin staining and germ layer-specific antibody detection)

## Proliferation assay

They were performed using MTT assay (M2128 Sigma) according to manufacturers instructions. MnSCs were plated at a density of 25.000 cells/24 well plate, and 570nm absorbance was measured at the days indicated using a microplate reader. Experiments were done in triplicates.

## qRT-PCR assay

RNA was isolated using RNeasy kit (Qiagen) according to manufacturer´s protocol. First-strand cDNA was primed via oligodT oligonucleotides and RT-PCR was performed with primer sets described at key resource table. For quantitative RT-PCR, brilliant SYBR green (Biorad) was used.

To determine differences in EB differentiation capacity, we used the Thermofisher's Taqman hPSC Scorecard Panel array (Bock et al., 2011). The array derives an algorithmic comparison of input pluripotent and EB differentiated iPSCs to its reference set of data that is comprised of the methylation status of genes and their expression levels found in (differentiated/undifferentiated) 20 ESC and 12 iPSC.

## Immunostaining

Cells were fixed in 4% (w/v) paraformaldehyde (Sigma-Aldrich) in PBS for 15 min and blocked in 5% goat serum with 0.3% (v/v) Triton-X-100 (Sigma-Aldrich) for 1 h. Blocking buffer:PBS (1:2) was used to dilute primary antibodies (listed above). Secondary antibodies coupled to fluorescent dies (Life Technolgies) were incubated at room temperature for 45 min at 1:500. Nuclei were stained with either Hoechst 33342 (Thermo Scientific) or 4,6-diamidino-2-phenylindole (DAPI; Sigma-Aldrich). Fluorescence images were acquired using a Leica SP5 II confocal system or a Leica 6000B epifluorescence microscope.

## Flow cytometry

After differentiation into cardiomyocytes or pancreatic progenitors, cells were dissociated with TrypLE Select (Gibco) for 5–10 min and neutralized with DMEM containing 10% foetal bovine serum. Thereafter, the cells were fixed with 4% (w/v) paraformaldehyde for 30 min at 4°C. Then, the fixed cells were stained with the cardiac troponin T (cTnt), or normal mouse IgG

(Santa Cruz Biotechnology, Inc.) in perm/wash buffer (Becton Dickinson). Intracellular staining of PDX-1 required cell permeabilization (Cytofix/Phosflow™ perm buffer III, Becton Dickinson, BD, Franklin Lakes, NJ, USA). Alexa Fluor 488-conjugated donkey anti-mouse IgG (Life Technologies) was used as a secondary antibody. The stained cells were analyzed using a flow cytometer (Beckman Coulter Gallios). Data were analyzed using Kaluza Beckman Coulter.

Co-immunoprecipitation and western blot assay

Two million MnSCs transduced with the different factors were used for each immunoprecipitation assay 72 hours after transduction. For SOX15 immunoprecipitation, cell pellets were washed twice with PBS before cell lysis. For immunoprecipitation, 1 mg of cell lysate (200 μl) was diluted to 500 μl in lysis buffer M-PER® Mammalian Protein Extraction Reagent (Thermo Scientific) containing protease inhibitors and incubated with 5ul of sheep anti-SOX15 or equivalent amount of sheep IgG overnight at 4ºC. Following overnight incubation stable complexes were affinity purified by incubation with 50 ml of Protein-G dynobeads (Invitrogen-Life Technologies) for 6 hours at 4ºC. Beads bound to immunoprecipitated complexes were washed once in lysis buffer and twice in PBS. Bound proteins were eluted from the beads by boiling in 2X Laemmli buffer and size fractionated using SDS-PAGE. Desired protein was detected by Western blot analysis using an affinity purified antibody. For SOX15, ASF1A and GAPDH western blot cells were washed with ice-cold PBS and lysed in 1% Igepal buffer (50 mM HEPES pH 7.4, 10 mM EDTA, 150 mM NaCl, 10 mM sodium pyrophosphate, 100 mM sodium fluoride, 1 mM sodium vanadate and a tablet of C-complete (Roche) protease inhibitor cocktail. After centrifugation at 12,000 x g for 15 min, 100ug of protein supernatant was resuspended in Laemmli SDS-DTT sample buffer for western blot analysis using the specific antibodies.

Gene Expression Analysis

Global gene expression profiles of somatic and pluripotent cells were obtained using Illumina Human HT-12 v4.0 Expression BeadChip (San Diego, CA) covering well-characterized genes, gene candidates, and splice variants with over 47,000 probes. Raw data were exported from Illumina GenomeStudio to an R session. Limma package (Ritchie et al., 2015) was used to correct the background with the NormExp method (McGee and Chen, 2006) and to apply

quantile normalization. Probes with detection P-value > 0.05 in at least 5 % of samples were removed. The expression of those genes with more than one probe was calculated as the median value of all their probes.

Differential gene expression analysis was done applying linear models implemented limma (Ritchie et al., 2015). For each comparison we selected those genes with P-value adjusted by False Discovery Rate (FDR) < 0.05 and absolute log fold change (FC) > 2. Euclidean distance measure and the complete agglomeration method were used to perform the hierarchical clustering.

Gene Ontology (GO) analysis was done using The Gene Ontology Resource (GO-enrichment analysis, which indentified biologically-relevant categories that are over-represented in the input gene set (Ashburner et al., 2000; The Gene Ontology, 2019). EASE identifies GO categories in the input gene list that are over-represented using jackknife iterative resampling of Fisher exact probabilities, with Bonferroni multiple testing correction. The "EASE score" is the upper bound of the distribution of Jackknife Fisher exact probabilities, which is a significance level with smaller EASE scores indicating increasing confidence in overrepresentation. We picked GO categories that have EASE scores of 0.05 or lower as significantly over-represented. Pathway analysis was done using Ingenuity Software Knowledge Base (IKB), (Redwood City, CA) to identify pathways that are significantly activated for a given input gene list. The association P-value between an input gene list and a known pathway is calculated using right-tailed Fisher Exact Test. We picked pathways that had a FDR < 0.05.

Global gene expression profiles of somatic cells five days after specific combination transduction were obtained after RNA extraction and quality analysis (Bioanalyzer 2100-Agilent). cDNA was synthesized, labelled with biotin and hybridized with independent Human Clarion-S Microarrays (Affymetrix) following Affymetrix protocol. Microarrays were scanned with Affymetrix GeneChip Scanner 7G, and the obtained data were analyzed with Affymetrix ® GeneChip® Command Console® 2.0 software. The microarray expression dataset is publicly available at the GEO repository. Further analyses were performed using the Transcriptome Analysis Console (TAC, Affymetrix) v4.0 10 software and R version 3.5.0.

Methylation analysis.

DNA was purified (QIAGEN Gentra Puregene Cell Kit), quantified (Qubit dsDNA BR Assay Kits, Life Technologies) and bisulphite-converted (EZDNA Methylation Kit, Zymo Research) according to the manufacturer's protocol. Bisulphite-converted DNA was hybridized to the Infinium HumanMethylation 450K beadchip (Illumina) and scanned on a HiScan (Illumina). All samples passed GenomeStudio (Illumina) quality-control steps based on built-in control probes.

Data obtained from our eleven samples were combined with four MSC (1-4), four hADF and three BM-MSC cell lines and five iPS cell lines from each MnSC donor for each reprogramming method OSK or AOX15 and 3 cell hESC lines for hierarchical clustering. We performed processing, normalization and differential methylation analysis using the statistical programming language R (http://www.r-project.org/) and the R package RnBeads (Assenov et al., 2014) with default parameters. Global DNA methylome analysis was performed at CpG level.

Violin plots showing global methylation patterns for each population were generated with ggplot2 R package (Wickham, 2009) averaging the methylation values from all samples of each population. To test if differences in these global methylation patterns are statistically significant we used GAMP R package (Zhao et al., 2015).

**Quantification and statistical analysis**

Statistical analyses were performed in GraphPad Prism 7 using Student's t test or a one-way ANOVA with TUKEY post hoc test where appropriate. Significance and the value of replicates used are indicated in each figure legend *$p < 0.05$; **$p < 0.01$, ***$p < 0.005$. The data are presented as the mean ± SEM.

**Key Resources Table:**

| REAGENT or RESOURCE | SOURCE | IDENTIFIER |
|---|---|---|
| Antibodies | | |
| goat anti-OCT4 (IF assays) | Santa Cruz Biotechnology | Cat#sc-8628 |
| mouse anti-OCT4 (Wb assays) | Santa Cruz Biotechnology | Cat#sc-5279 |
| rabbit anti-NANOG | Santa Cruz Biotechnology | Cat#sc-33760 |

| rabbit anti LIN-28 | Santa Cruz Biotechnology | Cat#sc-67266 |
|---|---|---|
| mouse anti Brachyury | Santa Cruz Biotechnology | Cat#sc-166962 |
| mouse anti-GATA4 | Santa Cruz Biotechnology | Cat#sc-25310 |
| mouse anti-KLF4 | Santa Cruz Biotechnology | Cat#sc-393462 |
| rabbit anti SOX15 (IF assays) | Santa Cruz Biotechnology | Cat#sc-20101 |
| mouse anti TpnT | Santa Cruz Biotechnology | Cat#sc-20025 |
| mouse anti PDX1 | Santa Cruz Biotechnology | Cat#sc-390792 |
| rabbit anti-ASF1A | Cell Signalling Technology | Cat#2990 |
| sheep anti SOX15 (IP and Wb assays) | R&D Systems | Cat#af4070 |
| rabbit anti-SOX2 | Abcam | Cat#AB5603 |
| rabbit anti-DDX4 (VASA | Abcam | Cat#ab13840 |
| mouse anti Nestin | Abcam | Cat#ab22035 |
| mouse anti-TRA-1-60 | Chemicon/Millipore | Cat#MAB4360 |
| mouse anti TRA-1-60 StainAlive | STEMGEN | Cat#09-0068 |
| mouse anti-b-ACTIN | Sigma-Aldrich | Cat#A5316 |
| rabbit anti GAPDH | Cusabio | Cat#CSB-PA00025A0Rb |
| rabbit anti PAX-6 | Biolegend | Cat#901301 |
| mouse anti Tuj1 | Covance | Cat#MMS-435P |
| mouse anti-SSEA4 | Developmental Studies Hybridoma bank (Iowa) | Cat#MC-813-70 |
| rabbit anti-PRMT5 | Sigma-Aldrich | Cat#07-405 |
| rabbit anti-AFP | Agilent-DAKO | Cat#IR500 |
| rabbit anti-αSMA | Agilent-DAKO | Cat#IR611 |
| Alexa Fluor® 488 donkey anti mouse IgG (H+L) | Life Technologies | Cat#A21202 |
| Alexa Fluor® 488 donkey anti rabbit IgG (H+L) | Life Technologies | Cat#A21206 |
| Alexa Fluor 555 donkey anti-rabbit IgG (H+L) | Life Technologies | Cat#A31572 |
| Alexa Fluor 555 donkey anti-mouse IgG (H+L) | Life Technologies | Cat#A31570 |
| Alexa Fluor® 488 donkey anti-goat IgG (H+L) | Life Technologies | Cat#A11055 |
| Peroxidase AffiniPure Goat Anti-Rabbit IgG (H+L) | Jackson InmunoResearch | Cat#111-035-144 |
| Peroxidase AffiniPure Goat Anti-Mouse IgG (H+L) | Jackson InmunoResearch | Cat#115-035-003 |
| | | |
| | | |
| **Bacterial and Virus Strains** | | |
| | | |
| pMXs-GFP | Cell Biolabs, INC | Cat#RTV-053 |
| pMXs-hOCT4 | (Takahashi et al., 2007) | Addgene-Cat#17217 |
| pMXs-hSOX2 | (Takahashi et al., 2007) | AddgeneCat#17218 |
| pMXs-hKLF4 | (Takahashi et al., 2007) | AddgeneCat#17219 |
| pMXs-hcMYC | (Takahashi et al., 2007) | Addgene Cat#17220 |

| pMXs-hASF1A | (Gonzalez-Munoz et al., 2014) | Supplied after request |
|---|---|---|
| pMXs-SOX15 | This work | N/A |
| gag/pol | (Reya et al., 2003) | Addgene Cat#14887 |
| pCMV-VSV-G | (Stewart et al., 2003) | Addgene Cat#8454) |
| | | |
| **Chemicals, Peptides, and Recombinant Proteins** | | |
| | | |
| KO_DMEM | Thermo Fisher Scientific | Cat#10829018 |
| Alpha-minimum essential medium (α-MEM) | Sigma Aldrich | Cat#M4526-500ML |
| DMEM/F12 | Thermo Fisher Scientific | Cat#11320-082 |
| MEM Non-Essential Amino Acids Solution (100X) | Thermo Fisher Scientific | Cat#11140068 |
| L-Glutamine | Thermo Fisher Scientific | Cat# 21051024 |
| Penicillin-Streptomycin | Thermo Fisher Scientific | Cat# 15070063 |
| 2-mercaptoethanol | Thermo Fisher Scientific | Cat# 21985023 |
| Fetal Bovine Serum, Regular (Heat Inactivated) | Corning | Cat# 35-011-CV |
| KO-Serum Replacement | Thermo Fisher Scientific | Cat# 10828028 |
| 2-mercaptoethanol | Thermo Fisher Scientific | Cat# 21985023 |
| Recombinant human basic FGF-premium grade | MACS-Miltenyi Biotec | Cat#130-093-843 |
| Y-27632 | Tocris Biosciences | Cat# 1254 |
| Matrigel hESC-qualified matrix | Corning | Cat# 354277 |
| Recombinant Human Wnt-3a Protein | R&D Systems | Cat#:5036-WN |
| Recombinant Human BMP-4 Protein | R&D Systems | Cat#:314-BP/CF |
| STEMdiff™ Cardiomyocyte Differentiation Kit | STEMCELL Technologies | Cat #05010 |
| STEMdiff™ Pancreatic Progenitor Kit | STEMCELL Technologies | Cat#05120 |
| Gelatin Solution | Sigma-Aldrich | Cat#G1393 |
| Human Mesenchymal Stem Cell Functional Identification Kit | R&D Systems | Cat#SC006 |
| Epidermal growth factor (EGF) | Peprotech | Cat#AF-100-15 |
| StemPro NSC SFM Supplement | Life Technologies | Cat#A1050901 |
| GDF9 human recombinant | Sigma-Aldrich | Cat#SRP4872 |
| Accutase solution | Sigma-Aldrich | Cat# A6964-100ML |
| Polybrene | Sigma-Aldrich | Cat#H9268-10G |
| Venor GeM Classic | Minerva Biolabs | Cat#11-1050 |
| Histopaque 1077 | Sigma-Aldrich | Cat#10771-100ML |
| Ficoll hypaque | Sigma-Aldrich | Cat#GE17-1440-02 |
| N-2 Supplement (100X) | Thermo Fisher Scientific | Cat# 17502048 |
| B-27 Supplement (50X), minus vitamin A | Thermo Fisher Scientific | Cat# 12587010 |
| GlutaMAX™ Supplement | Gibco-ThermoFisher | Cat# 35050061 |
| Lysis buffer M-PER® Mammalian Protein Extraction Reagent | Thermo Scientific | Cat# 78501 |
| Dynabeads Protein G | Life Technologies | Cat#:10004D |
| Sheep IgG Isotype Control | Thermo Fisher Scientific | Cat# 31243 |
| cOmplete™ Protease Inhibitor Cocktail | MERCK | Cat#11697498001 |
| Igepal (Nodidet P40 subsitute) | MERCK | Cat#11332473001 |
| DAPI | Sigma-Aldrich | Cat#D9542 |
| RIPA | Sigma-Aldrich | Cat#:R0278 |
| BSA | Sigma-Aldrich | Cat#:A4503 |

| Paraformaldehyde | Electron Microscopy Sciences | Cat#:15710 |
|---|---|---|
| DPBS | Corning | Cat#:21-031-CM |
| Donkey Serum | Equitech-Bio | Cat#:SD30-0500 |
| Triton X-100 | Fisher Scientific | Cat#:BP151-500 |
| Normal Donkey Serum | Sigma Aldrich | Cat#D9663 |
| | | |
| **Critical Commercial Assays** | | |
| | | |
| SYBR Green PCR Master Mix | Applied Biosystems | Cat#4309155 |
| BCA Assay | Thermo Fisher | Cat#23227 |
| QIAGEN Gentra Puregene Cell Kit | QIAGEN | Cat#: 158388 |
| RNeazy Mini Plus Kit QIAGEN | QIAGEN | Cat# 74136 |
| Qubit dsDNA BR Assay Kits | Life Technologies | Cat#Q32853 |
| EZDNA Methylation Kit | Zymo Research | Cat#D5003 |
| Human Clarion-S Microarrays Affymetrix | Applied Biosystems | Cat#902927 |
| Illumina Human HT-12 v4.0 Expression BeadChip | Illumina | Cat#Human HT-12 v4.0 |
| Infinium HumanMethylation 450K beadchip (Illumina) | Illumina | Cat#WG-314-1003 |
| MTT assay | Sigma Aldrich | Cat#M2128 |
| | | |
| **Deposited Data** | | |
| RNA-array of hADFs, MnSCs, BM-MSCs, hESCs, OSK-iPSCs, and AOX15-iPSCs | This paper | GSE139085 and a temporal private token mvoliyssxrkjdgd |
| methylation-arrays of hADFs, MnSCs, BM-MSCs, hESCs, OSK-iPSCs, and AOX15-iPSCs | This paper | GSE139085 and a temporal private token mvoliyssxrkjdgd |
| | | |
| **Experimental Models: Cell Lines** | | |
| Human: HEK293T/17 cells ATCC Cat# CRL | 11268; RRID: CVCL_1926 | Human: HEK293T/17 cells ATCC Cat# CRL |
| Human: Passage 33 and 67 H9 human ES | WiCell Research Institute | Cat#WA09 |
| Human: Passage 40 H1human ES | WiCell Research Institute | Cat#WA01 |
| Human female donor 01: adult dermal fibroblasts_donor-01 | This study | hADF-01 |
| Human female donor 02: adult dermal fibroblasts_donor-02 | This study | hADF-02 |
| Human female donor 03: adult dermal fibroblasts_donor-03 | This study | hADF-03 |
| Human female donor 04: adult dermal fibroblasts_donor-04 | This study | hADF-04 |
| Human female donor 01: adult menstrual derived stromal cells_donor01 | This study | MnSC-01 |

| | | |
|---|---|---|
| Human female donor 02: adult menstrual derived stromal cells_donor02 | This study | MnSC-02 |
| Human female donor 03: adult menstrual derived stromal cells_donor03 | This study | MnSC-03 |
| Human female donor 04: adult menstrual derived stromal cells_donor04 | This study | MnSC-04 |
| Human female donor 01: adult bone marrow mesenchymal stem cells_donor01 | This study | BM-MSC-01 |
| Human female donor 02: adult bone marrow mesenchymal stem cells_donor02 | This study | BM-MSC-02 |
| Human female donor 03: adult bone marrow mesenchymal stem cells_donor03 | This study | BM-MSC-03 |
| OSK-iPSC-01,-02,-03,-04 (from MnSC -01 to -04) passage 25-28 | This study | N/A |
| AOX15-iPSC--01,-02,-03,-04 (from MnSC -01 to -04) passage 25-28 | This study | N/A |
| | | |
| | | |

**Experimental Models: Organisms/Strains**

| | | |
|---|---|---|
| NOD SCID Mouse Congenic Immunodeficient | Charles River | NOD.CB17-Prkdcscid/NCrCrl |
| | | |

**Oligonucleotides**

| | Forward | Reverse |
|---|---|---|
| | | |
| SOX15 cloning | ggcgctttgTTTAAACCCggCACCATg**GCGCTACCAGGCTCCTCACA** | GGCCGAAGGGTTTAAAccctca**GAGGTGGGTTAGGGGCATGG** |
| RT POU5F1 endog | CCTCACTTCACTGCACTGTA | CAGGTTTTCTTTCCCTAGCT |
| RT POU5F1 transgene | CCCCAGGGCCCCATTTTGGTACC | CTTCCCTCCAACCAGTTGCCCCAAAC |
| RT POU5F1 | GGTTCTATTTGGGAAGGTAT | CATGTTCTTGAAGCTAAGC |
| RT ASF1A transgene | TTTAAACCCggCACCatggca | GCATCTGCATCTGGAATGAG |
| RT ASF1A | CCGCAGGAAGGCATATGTT | GCATCTGCATCTGGAATGAG |
| RT SOX15 transgene | CCggCACCATgATGGCGCTACCAG | GAGCTCCACACCATGAACG |
| RT SOX15 | CCCATGCTACTCGACAGCCTACAG | TGGAGCCTAGGGTCACTCTG |
| RT-ACTIN | TGAAGTGTGACGTGGACATC | GGAGGAGCAATGATCTTGAT |
| RT-GAPDH | ATGGAAATCCCATCACCATCTT | CGG CCC ACT TGA TTT TGG |
| RT-TBP | CGGCTGTTTAACTTCGCTTC | CACACGCCAAGAAACAGTGA |
| RT-hTERT | TGTGCACCAACATCTACAAG | GCGTTCTTGGCTTTCAGGAT |
| RT-hGDF3 | AAATGTTTGTGTTGCGGTCA | TCTGGCACAGGTGTCTTCAG |
| RT-SOX2 | CCCAGCAGACTTCACATGT | CCTCCCATTTCCCTCGTTTT |
| RT-KLF4 | GATGAACTGACCAGGCACTA | GTGGGTCATATCCACTGTCT |
| RT-DNMT3B | ATAAGTCGAAGGTGCGTCGT | GGCAACATCTGAAGCCATTT |
| RT-NANOG | TACCTCAGCCTCCAGCAGAT | TCTGGAACCAGGTCTTCACC |

| | | |
|---|---|---|
| RT-REX1 | CCCACAGTCCATCCTTACAGAGTT | GGG ACT TTG CCC CCA AAC |
| RT-DPPA3 | GTTACTCGGCGGAGTTCGTA | TGAAGTGGCTTGGTGTCTTG |
| RT-RUNX1 | CCCTAGGGGATGTTCCAGAT | TGAAGCTTTTCCCTCTTCCA |
| RT- BRACHYURY | ACCACCGCTGGAAATATGTGAACG | AACTCTCACGATGTGAATCCGAGG |
| RT-NESTIN | CAGCGTTGGAACAGAGGTTGG | TGGCACAGGTGTCTCAAGGGTAG |
| RT-AFP | AGCTTGGTGGTGGATGAAAC | CCCTCTTCAGCAAAGCAGAC |
| RT-NCAM | ATGGAAACTCTATTAAAGTGAACCTG | TAGACCTCATACTCAGCATTCCAGT |
| RT-PAX6 | CGGAGTGAATCAGCTCGGTG | CCGCTTATACTGGGCTATTTTGC |
| RT-GATA4 | CTCTACATGAAGCTCCAC | CTGCTGGTGTCTTAGATT |
| RT-NKX2.5 | ACCCTGAGTCCCCTGGATTT | TCACTCATTGCACGCTGCAT |
| RT-αMHC | TCTCCGACAACGCCTATCAGTAC | GTCACCTATGGCTGCAATGCT |
| RT-MEF2C | TAACTTCTTTTCACTGTTGTGCTCCTT | GCCGCTTTTGGCAAATGTT |
| RT-MLC2A | CAGGCCCAACGTGGTTCTT | CCATCACGATTCTGGTCGATAC |
| RT-PDX1 | CGTCCAGCTGCCTTTCCCAT | CCGTGAGATGTACTTGTTGAATAGGA |
| RT-NKX6.1 | GGGCTCGTTTGGCCTATTCGTT | CCACTTGGTCCGGCGGTTCT |
| RT-SOX9 | GACCAGTACCCGCACTTG | GCTCTCGTTCAGAAGTCTC |
| RT-HNF6- | GGACCTCAAGATAGCAGGTTTAT | CAGAATGCAGGTGAGCTAAGT |
| RT-FOXA2- | GGGAGCGGTGAAGATGGA | TCATGTTGCTCACGGAGGAGTA |
| RT-VASA | GATGTTCCTGCATGGTTGGA | CCATGACTCATCATCTACTGGA |
| RT-bLIMP/PRMD1 | TTCTTGTGTGGTATTGTCG | TCTCTTTGGGACATTCTTT |
| RT-DAZL | ACACTGAAACTTATATGCAGCC | CGGAGGTACAACATAGCTCCTT |
| RT-Stella | GGAGTTAAGAAGGAATCA | AAGATTTATGGCTGAAGT |
| RT-DMRT1 | CTTGGAGTAACAGGCTTATTC | CGTTCTCAACAGTTAAGATAGTAT |
| RT-NANOS3 | CTACACCTCCGTCTACAG | GTGTCTTCGCCTTGTCAG |
| RT-PRMT5 | TTAATCAGGAAGATAACACca | GCATTCTCAATTATATCATCtct |
| | | |

**Recombinant DNA**

| | | |
|---|---|---|
| cDNAs encoding human SOX15 | Open Biosystems | Cat# IHS1380-97434272 |
| | | |

**Software and Algorithms**

| | | |
|---|---|---|
| | | |
| Affymetrix ® GeneChip® Command Console® 2.0 software | Affymetrix (Thermo Fisher) | N/A |
| R package limma v3.32.3 | (Ritchie et al., 2015) | https://bioconductor.org/packages/release/bioc/html/limma.html |
| R package RnBeads | (Assenov et al., 2014) | https://bioconductor.org/packages/release/bioc/html/RnBeads.html |

| Ggplot2 R package | (Wickham, 2009) | https://www.bioconductor.org/packages/devel/bioc/vignettes/sights/inst/doc/sights.html |
|---|---|---|
| GAMP R package | (Zhao et al., 2015). | http://bioconductor.org/packages/release/bioc/html/methylPipe.html |
| | | |

## Supplemental References

Ashburner, M., Ball, C.A., Blake, J.A., Botstein, D., Butler, H., Cherry, J.M., Davis, A.P., Dolinski, K., Dwight, S.S., Eppig, J.T., et al. (2000). Gene ontology: tool for the unification of biology. The Gene Ontology Consortium. Nat Genet 25, 25-29.

Assenov, Y., Muller, F., Lutsik, P., Walter, J., Lengauer, T., and Bock, C. (2014). Comprehensive analysis of DNA methylation data with RnBeads. Nat Methods 11, 1138-1140.

Bock, C., Kiskinis, E., Verstappen, G., Gu, H., Boulting, G., Smith, Z.D., Ziller, M., Croft, G.F., Amoroso, M.W., Oakley, D.H., et al. (2011). Reference Maps of human ES and iPS cell variation enable high-throughput characterization of pluripotent cell lines. Cell 144, 439-452.

Byrne, J.A., Nguyen, H.N., and Reijo Pera, R.A. (2009). Enhanced generation of induced pluripotent stem cells from a subpopulation of human fibroblasts. PLoS One 4, e7118.

Casado-Diaz, A., Santiago-Mora, R., Jimenez, R., Caballero-Villarraso, J., Herrera, C., Torres, A., Dorado, G., and Quesada-Gomez, J.M. (2008). Cryopreserved human bone marrow mononuclear cells as a source of mesenchymal stromal cells: application in osteoporosis research. Cytotherapy 10, 460-468.

Chang, E.A., Beyhan, Z., Yoo, M.S., Siripattarapravat, K., Ko, T., Lookingland, K.J., Madhukar, B.V., and Cibelli, J.B. (2010). Increased cellular turnover in response to fluoxetine in neuronal precursors derived from human embryonic stem cells. Int J Dev Biol 54, 707-715.

Delcroix, G.J., Curtis, K.M., Schiller, P.C., and Montero-Menei, C.N. (2010). EGF and bFGF pre-treatment enhances neural specification and the response to neuronal commitment of MIAMI cells. Differentiation 80, 213-227.

Gonzalez-Munoz, E., Arboleda-Estudillo, Y., Otu, H.H., and Cibelli, J.B. (2014). Cell reprogramming. Histone chaperone ASF1A is required for maintenance of pluripotency and cellular reprogramming. Science 345, 822-825.

Hermann, A., Liebau, S., Gastl, R., Fickert, S., Habisch, H.J., Fiedler, J., Schwarz, J., Brenner, R., and Storch, A. (2006). Comparative analysis of neuroectodermal differentiation capacity of human bone marrow stromal cells using various conversion protocols. J Neurosci Res 83, 1502-1514.

Kee, K., Angeles, V.T., Flores, M., Nguyen, H.N., and Reijo Pera, R.A. (2009). Human DAZL, DAZ and BOULE genes modulate primordial germ-cell and haploid gamete formation. Nature 462, 222-225.

Leng, L., Tan, Y., Gong, F., Hu, L., Ouyang, Q., Zhao, Y., Lu, G., and Lin, G. (2015). Differentiation of primordial germ cells from induced pluripotent stem cells of primary ovarian insufficiency. Hum Reprod 30, 737-748.

Long, X., Olszewski, M., Huang, W., and Kletzel, M. (2005). Neural cell differentiation in vitro from adult human bone marrow mesenchymal stem cells. Stem Cells Dev 14, 65-69.

McGee, M., and Chen, Z. (2006). Parameter estimation for the exponential-normal convolution model for background correction of affymetrix GeneChip data. Stat Appl Genet Mol Biol 5, Article24.

Reya, T., Duncan, A.W., Ailles, L., Domen, J., Scherer, D.C., Willert, K., Hintz, L., Nusse, R., and Weissman, I.L. (2003). A role for Wnt signalling in self-renewal of haematopoietic stem cells. Nature 423, 409-414.

Ritchie, M.E., Phipson, B., Wu, D., Hu, Y., Law, C.W., Shi, W., and Smyth, G.K. (2015). limma powers differential expression analyses for RNA-sequencing and microarray studies. Nucleic Acids Res 43, e47.

Stewart, S.A., Dykxhoorn, D.M., Palliser, D., Mizuno, H., Yu, E.Y., An, D.S., Sabatini, D.M., Chen, I.S., Hahn, W.C., Sharp, P.A., et al. (2003). Lentivirus-delivered stable gene silencing by RNAi in primary cells. RNA 9, 493-501.

Takahashi, K., Tanabe, K., Ohnuki, M., Narita, M., Ichisaka, T., Tomoda, K., and Yamanaka, S. (2007). Induction of pluripotent stem cells from adult human fibroblasts by defined factors. Cell 131, 861-872.

The Gene Ontology, C. (2019). The Gene Ontology Resource: 20 years and still GOing strong. Nucleic Acids Res 47, D330-D338.

Wickham, H. (2009). ggplot2: Elegant Graphics for Data Analysis, Use R! Springer-Verlag, New York.

Zhao, N., Bell, D.A., Maity, A., Staicu, A.M., Joubert, B.R., London, S.J., and Wu, M.C. (2015). Global analysis of methylation profiles from high resolution CpG data. Genet Epidemiol 39, 53-64.